NASA Technical Memorandum 81583

Analysis of Pressure Spectra Measurements in a Ducted Combustion System

Jeffrey Hilton Miles
Lewis Research Center
Cleveland, Ohio

November 1980

NASA

TABLE OF CONTENTS

LIST OF FIGURES

LIST OF TABLES

I. INTRODUCTION

Sound is both a physical phenomenon defined as the wave oscillation of a medium and a physiological phenomenon defined as a sensation received by the ear due to acoustic waves. As a mechanical vibration sound is characterized by frequency, amplitude, and phase angle. However, no simple and unique relationship exists between the physical measurement of sound and the human perception of sound. Consequently, many physiological methods exist to evaluate various aspects of the perception of sound. For example, the human perception of pure tones is described by normal equal loudness contours.

Furthermore, sound is also a psychological phenomenon which can be characterized in terms of annoyance and desirability. An undesirable, unwanted, or excessive sound is called a noise. Besides producing annoyance, noise can produce various degrees of permanent hearing loss. Also, since people prefer to live in quiet places and to be near quiet objects, noise can have an economic importance.

Due to the increasing public concern with the environment and to the growth of commercial aviation in this country, aircraft noise is considered to be one of the more significant noise sources. As a result aircraft noise abatement is a major objective of government and industry.

Airport community noise can be reduced by applying restrictive aircraft and airport operational procedures or by developing new technology. Safety and economic considerations reduce the effectiveness of

such operational restrictions as the multi-segment approach, power cutback, runway restrictions, establishment of airport buffer zones, and land use control. Consequently, in recent years noise has become an important consideration in the design of turbofan aircraft engines.

In the study of turbofan aircraft engine noise, the noise is considered to be due to various sources and each source is associated with specific components of the engine or specific air flow conditions. The noise from turbofan engines is often attributed to the following three sources: the fan, the jet exhaust, and the engine core. Fan noise propagates to the ground from both the engine inlet and exit duct planes. Also, jet mixing noise is produced by both the fan and core exhaust air. These turbofan engine noise sources are shown schematically in Figure 1. The relative magnitude of fan noise and jet exhaust noise is generally greater than core noise for most operating conditions of current engines.

Fan noise is characterized by a high pitched whine produced by the rotating fan blades. The high velocity jet exhaust generates noise as it mixes with the relatively quiescent atmosphere. The term "core" noise refers to all the other noise sources including the following:

1. Combustion noise which is the noise associated with pressure fluctuations due to uneven burning
2. Entropy noise which is the noise due to nonuniformities in the expanding gases as they pass through the turbine stages and the exhaust nozzle
3. Rotating machinery noise due to the compressor and turbine
4. Flow noise due to air passing through ducts and over internal surfaces.

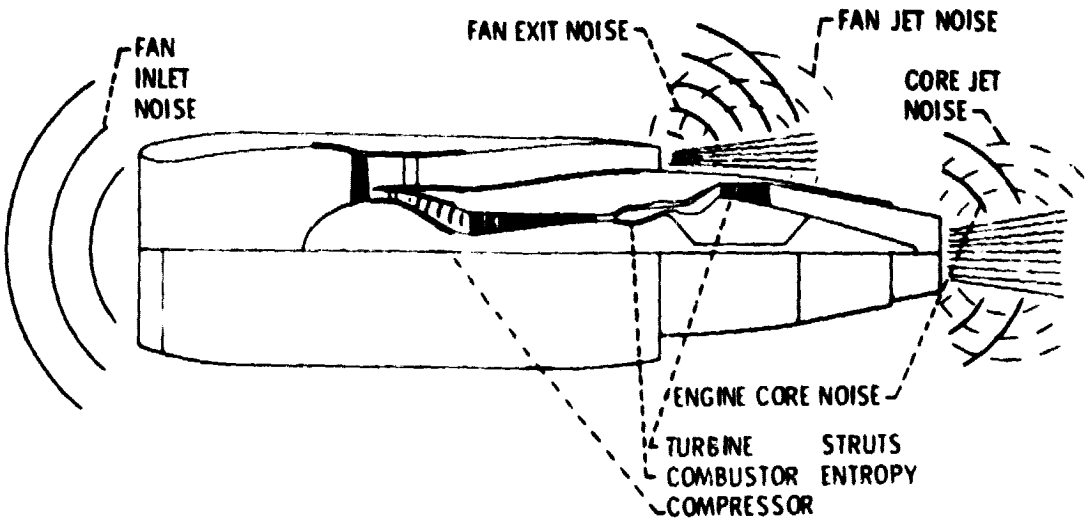

Figure 1. - Turbofan engine noise sources.

Most of the noise from current turbofan engines is attributed to the fan or jet. Over the past few years aircraft system quieting technology has been developed which reduces the noise from these two sources. However, research on core noise and combustion noise, in particular, has not been neglected.

Combustion noise research is conducted because it could be important in future aircraft design for three reasons. First, it could be the dominant noise source in the duct-burning turbofan engine, which is one of the proposed commercial supersonic aircraft engine propulsion systems (Stewart and Weber (1978)). Second, as the noise from the fan and jet sources is reduced on future aircraft, the importance of such secondary sources associated with the engine core as combustion noise increases. Third, core noise including combustion noise can be a significant contributor to overall engine noise during takeoff or approach when the fan noise and the jet noise are reduced because of forward velocity effects (Stone (1975)).

In order to characterize aircraft engine combustion noise the following items are of interest:

1. The acoustic power level variation with burner geometry and performance parameters
2. The transmission loss across the turbine and at the engine exit
3. The combustion noise directivity pattern of far field engine data
4. The combustion noise spectral shape
5. The peak frequency of the combustion noise spectrum.

These are also the items a combustion noise prediction scheme would yield as part of an aircraft engine design procedure.

In order to obtain this information, many different types of test facilities and a variety of measurement techniques are used to study combustion noise. These tests are conducted with the expectation that (1) combustion noise measurements on non-engine test facilities are related to combustion noise measurements on engine test facilities and (2) that combustion noise measurements made using different engines are related to one another. Some of these test facilities and measurement techniques will be described next.

The studies of Bonnell, Marshall, and Riecke (1971), Mathews and Rekos (1976), Karchmer and Reshotko (1976), Shivashankara (1977), Reshotko, Karchmer, Penko, and McArdle (1977), and Karchmer (1978) were made using operating turbofan engines.

Combustors installed in open flow ducts were used by Kazin and Emmerling (1974), Strahle, Muthukrishnan, and Neale (1977a, 1977b), Abdelhamid, Harrje, Plett, and Summerfield (1973), and Plett, Leshner, and Summerfield (1975).

The studies of Emmerling (1975), Emmerling and Bekofske (1976), Sofrin and Ross (1975), Sofrin and Riloff (1976), and Reshotko and Karchmer (1977) were made using combustors installed in closed duct systems called component development facilities.

Combustion noise from open flames was measured by Smith and Kelham (1963), Hurle, Price, Sugden, and Thomas (1968), Knott (1971), and Muthukrishnan, Strahle, and Handley (1976).

External and internal pressure measurements can be made on tests of combustors mounted in turbofan engines and in open flow ducts. Only internal pressure measurements can be made in tests of combustors in-

stalled in closed ducts, and only external pressure measurements can be made of the noise of open flames.

In the study of combustion noise, pressure measurements are subject to one-third octave band analysis or narrow band spectrum analysis to obtain frequency and amplitude information. Also, transfer function, correlation, and coherence calculations are sometimes made between pairs of pressure measurements to obtain information on amplitude and phase changes during propagation, on time delays between signals and on the signal to noise ratio.

Experimental studies of combustion noise using operating turbofan engines are made with realistic combustion region boundary conditions and at realistic combustion region operating conditions. However, separating combustion, fan, compressor, turbine, and jet noise contributions from one another in external far-field acoustic measurements can be difficult. Consequently, correlation and coherence techniques using internal and external microphones have been developed to identify combustion noise in the far-field acoustic measurements and to quantify its contribution (Karchmer and Reshotko (1976), Shivashankara (1977), Reshotko, Karchmer, Penko, and McArdle (1977), Karchmer, Reshotko, and Montegani (1977), Karchmer (1978)). Using these techniques, the combustor has been shown to be a source of low frequency core noise (Karchmer and Reshotko (1976), Karchmer, Reshotko, and Montegani (1977), Karchmer (1978)).

Extensive testing of many combustor designs on full-scale turbofan engines using correlation and coherence techniques can be expensive. An alternative procedure is to conduct acoustic design studies on a less expensive test facility. The combustor component duct rig is one type

of less expensive facility. Because this facility is closed, operating the combustor at realistic conditions of temperature, pressure, and flow is possible. However, the combustion region boundary conditions produced by a combustor component duct facility differ from those of an engine since the turbine is not included in the component duct rig. This may not be too significant since von Glahn (1978) was able to correlate combustor acoustic power levels inferred from internal fluctuating pressure measurements made on both the engine and the combustor component duct facilities with operating conditions and chamber geometries.

Constructing a combustor test facility which costs less than an engine can also be accomplished by installing a combustor in an open flow duct. For this facility also, the combustor boundary conditions differ from those of an engine. In addition, while the combustor in this type of facility can operate at turbofan engine combustor temperature and flow conditions, the combustor operating pressure for a given duct exit termination (horn, open duct, flange, nozzle) is also determined by the flow and temperature specified. Consequently, matching engine operating conditions with this rig is difficult. Therefore, the open flow duct rig is used more often in conducting such fundamental research as separating hydrodynamic entropy, and direct combustion noise contributions to internal fluctuating pressure measurement (Strahle, Muthukrishnan, and Neale (1977)) than in making parametric studies.

This disseration describes an investigation of the propagation of combustion noise in an open flow duct. This is a new area of research. The research is conducted using a combined experimental and

theoretical approach. The objective of the theoretical investigation is the study of the interaction of the combustion noise propagating in a plane wave mode with the duct combustion environment. In this case, the duct combustion environment includes the emissions produced by the combustor, the air flow, and the duct exit impedance and inlet impedance. The interaction of a propagating plane acoustic wave with combustor emissions has not previously been considered. This work uses a dynamic systems state-space approach to study this problem.

This investigation was initiated due to difficulties encountered in the study of the structure of the internal fluctuating pressure spectra measurements taken in an open flow combustion test facility. The structure of the measured spectra differed from the spectra predicted on the basis of longitudinal duct resonance mode theory using the combustor duct system exit temperature to determine the acoustic isentropic propagation velocity. However, the changes in the spectral structure when the geometry is changed longitudinally caused most investigators to conclude that the spectral structure is related to longitudinal duct resonance modes.

Since the spectral structure could not be understood, doubts arose about the usefulness of combustion data taken on a liquid fuel open flow combustion test facility. The money saved in using this type of facility for detailed study of combustion noise would be wasted if the experimental results could not be understood.

The work discussed herein is part of a research program at the NASA Lewis Research Center. The purpose of the research program is to analyze the pressure spectra measured within an operating ducted gas

turbine engine combustor test apparatus. The research program has the following major goals:

1. Identify the combustion noise source spectra
2. Identify the influence of the duct geometry on the spectra
3. Identify interactions between the combustion process and the acoustics.

This dissertation has the more limited goal of modeling the operating ducted combustion system and calculating pressure auto-spectra and cross-spectra. Consequently, only topics related to the propagation of combustion noise in a ducted system are studied.

In Chapter II, the failure of the use of the isentropic sound propagation velocity to predict the frequencies of longitudinal duct resonance modes in an operating ducted liquid fuel combustion system is explained. It is shown that liquid hydrocarbon droplets or solid soot particle emissions from a combustor may make the plane wave propagation velocity less than the isentropic speed of sound and may attenuate core noise. Any variation in plane wave propagation speed may have important consequences in the design and selection of acoustical duct lining to attenuate engine core noise. This variation in plane wave propagation velocity also implies that in order to predict the frequency variation of resonance caused peaks and dips in a combustion noise spectrum measured in a duct, one must measure soot and hydrocarbon emissions and understand the physics and chemistry of the acoustic emission interaction.

In the cases studied, the air mass flow rates are less than 2 kg/sec, the duct exit temperature is 920 K, and the flow Mach number is much less than unity. The type and amount of emissions depends on

such combustor operating conditions as the air and fuel mass flow rate and on the type of fuel. It also depends on combustor design of such items as swirlers and fuel nozzles. Since the problem is complex, only two fairly simple types of interactions between emissions and acoustics are treated herein. The interaction discussed occurs in a mixture of an ideal gas and either a cloud of liquid fuel droplets or a cloud of solid soot particles. In both cases, the interaction is between a plane wave propagating in the mixture and the cloud.

Smoke emissions are generated by aircraft engines (Jones (1977)). Consequently, the presence of a cloud of solid soot particles in a liquid fuel ducted combustor system is possible. Thus the selection of this case as one to be studied seems reasonable. The selection of the situation where the duct contains a cloud of liquid fuel droplets is more complicated.

In addition to smoke, aircraft engines also produce gaseous hydrocarbon pollution (Jones (1977)). Moreover, Jones (1977) says that under certain conditions where a combination of factors produces large drops and poor mixing of the air with the fuel spray high levels of hydrocarbons can be produced. The hydrocarbon gas pollution may be due to droplets which pass through the flame front without oxidizing and which eventually evaporate. Consequently, a cloud of liquid fuel droplets may exist in the ducted combustion system studied if droplets can pass through the flame front and if a typical droplet does not evaporate before it leaves the duct. For the cases studied a particle is in the duct less than 0.3 second. The calculation of the evaporation rate of a liquid fuel droplet is discussed by Graves and Bahr (1959), Faeth (1977), and Harrje (1972). Calculations are done using simplified

models. The results are a function of the initial conditions such as droplet diameter. Examination of some typical results showed that while the ambient temperature (920 K) is 300 to 400 K above the distillation temperature of the liquid, conditions could exist such that a liquid droplet might not evaporate completely in the time it is in the duct (Graves and Bahr (1959)). Accordingly, calculations were made considering the presence of a cloud of liquid fuel droplets.

The literature contains a number of theoretical and experimental studies of the propagation of a plane wave through a cloud of particles which show that particles can cause dispersion and attenuation. Studies considering viscous and thermal interaction but not mass transfer were made by Marble (1969), Epstein and Carhart (1953), and Chow (1964), Temkin and Dobbins (1966), and Dobbins and Temkin (1967). Studies which consider water vapor mass transfer in addition to viscous and thermal interaction were made by Cole and Dobbins (1970), Marble and Wooten (1970), Davidson (1975), and Marble and Candel (1975). The theory of Cole and Dobbins was experimentally confirmed by Cole and Dobbins (1971).

The physics of liquid hydrocarbon droplet attenuation is assumed to be identical to the physics of water droplet attenuation since the same physical models are used to describe droplet evaporation (Faeth (1977)). The approach followed in calculating liquid hydrocarbon droplet attenuation is similar to that of Marble and Candel (1975). The model for the physics and chemistry of carbon particle attenuation is handled by a modification of the theory given by Marble and Candel (1975). The consideration of mass transfer from the soot particle to the gas by particle oxidation is new.

In the approach used, the particle spacing is assumed to be small enough in comparison with the acoustic wavelength that the particle phase may be represented as a continuous distribution of weak acoustic source and dipoles. This is the approach used by Marble and Candel (1975) and a similar approach was previously used by Temkin and Dobbins (1966), Marble and Wooten (1970), and Davidson (1975). The method is popular since it shows explicitly the relaxation character of the problem and includes the dispersion of sound.

In Chapter III, a linear analytic procedure for modeling the combustion duct system acoustics is discussed. The model includes both the source region governed by the solution to a non-homogeneous wave equation and the propagation region governed by the solution to the homogeneous wave equation. All non-linear processes in the system such as those which might arise due to interaction of the pressure wave and the emissions are neglected in the model.

A solution to the Sturm-Liouville non-homogeneous one-dimensional wave equation, which governs the source region when there is no mean uniform flow, can be found by the method of eigenfunctions (Morse and Feshback (1973, p. 793), Byron and Fuller (1970)), or by construction of the one-dimensional Green's function (Morse and Feshback (1973, pp. 122 , 523, 825, 828, and 832), Duff and Naylor (1966)). Applications of both solution approaches to aero-acoustics are discussed by Goldstein (1976). The eigenfunction solution method was applied to a combustion source problem by Mailing (1963). The hon-homogeneous one-dimensional wave equation cannot be classified as being a Sturm-Liouville type if flow is included since this introduces complex coefficients into the wave equation. In the analysis developed in Chapter III, the presence

of a uniform mean duct flow and the interaction of the flow with combustion emissions is included, and the solution approach is based on construction of the one-dimensional Green's function.

A solution to the homogeneous one-dimensional wave equation which governs the propagation of plane waves in the duct is formulated as a two-port transmission line using acoustic transmission matrices. The use of this approach to model distributed parameter systems is discussed by Takahashi, Robbins, and Auslander (1972), and an introduction to its use in acoustics is given by Lampton (1978). The equations developed by Lampton (1978) are for the no-flow case. Transmission matrices which include flow have been previously applied to duct acoustic problems by Parrott (1973).

In Chapter IV, the experimental results are presented. In Chapter V, the experimental results are compared with the theory developed in Chapter III.

In summary, this dissertation analyzes dispersion in an operating liquid fuel ducted combustion system, gives a procedure for calculating pressure auto-spectra and cross-spectra, presents measured auto-spectra and cross-spectra, and compares the measured spectra with the calculated spectra.

II. PHYSICAL CONSIDERATIONS

In this chapter the propagation of a plane wave through a stationary gas containing a particle cloud of either liquid fuel droplets or solid soot particles is discussed. However, the governing equations will be derived for the more general case of non-zero mean velocity since the next chapter considers this case. At an appropriate point in this chapter the additional assumption of zero mean velocity will be made.

A. Governing Equations

The propagation of a plane wave through a gas containing liquid water droplets or solid soot particles is governed by a wave equation. The wave equation used in this chapter was derived by considering a plane wave propagating through a droplet or particle cloud in a stationary gas. This wave equation was derived by Marble and Candel (1975) for a cloud of water droplets. This section reviews the derivation and interpretation of this wave equation.

The wave equation derivation is based on the following major assumptions:

(1) The particulate mass fraction and volume fraction are small.

(2) The particulate spacing is smaller than the acoustic wavelengths considered. Consequently, the particle cloud and gas can be treated as a continuum.

(3) The fluctuations of pressure, density, temperature, entropy, and velocity are small compared with their mean values. Therefore, the squares and cross products of these parameters can be neglected.

(4) The fluid velocity is much smaller than the speed of sound.

(5) The bulk gas can be treated as an ideal gas.

In deriving the one-dimensional, constant area continuity equation, the liquid droplets or soot particles are assumed to be mass sources. Consequently, the density of the gas and the gas velocity are related in the continuity equation

$$\partial\bar{\rho}/\partial\theta + \partial(\overline{\rho u})/\partial x = n\bar{\phi} \qquad (2.1.1)$$

where $\bar{\rho}$ is the gas density, $\bar{u}$ is the gas velocity, θ is time, x is a Cartesian coordinate, and $n\bar{\phi}$ is the local mass production rate due to the presence of n particles per unit volume each having a rate of mass production of $\bar{\phi}$. (The symbols used in this chapter are defined at the end of the chapter.)

The momentum equation for the gas is

$$\partial(\overline{\rho u})/\partial\theta + \partial(\overline{\rho u^2})/\partial x + \partial\bar{p}/\partial x = n\bar{F} + n\phi\bar{u}_p \qquad (2.1.2)$$

where $\bar{p}$ is the gas pressure. The first term on the right side of Eq. (2.1.2) represents a volumetric force due to the n particles per unit volume each exerting a drag force on the gas, $\bar{F}$, as the cloud of of particles moves through the gas. Using Stokes' drag law, the drag force is

$$\bar{F} = 6\pi r\mu(\bar{u}_p - \bar{u}) \qquad (2.1.3)$$

where r is the particle radius, μ is the gas dynamic viscosity, and $\bar{u}_p$ is the particle velocity. The second term on the right side of Eq. (2.1.2) represents the momentum added to the gas locally which is equal to the product of the mass generated and the local particle velocity $\bar{u}_p$. Substituting Eq. (2.1.1) into Eq. (2.1.2) yields

$$\bar{\rho}\partial\bar{u}/\partial\theta + \overline{\rho u}\,\partial\bar{u}\,\partial x + \partial\bar{p}/\partial x = n\bar{F} + n\bar{\phi}(\bar{u}_p - \bar{u}) \qquad (2.1.4)$$

The gas containing the particles is assumed to be a multicomponent ideal gas characterized by the following two equations:

$$\bar{p} = \bar{\rho}\mathcal{R}\bar{t}/(MW) \qquad (2.1.5)$$

and

$$\bar{e} = c_v\bar{t} \qquad (2.1.6)$$

where $\mathcal{R}$ is the gas constant, $\bar{t}$ is the temperature, (MW) is the gas molecular weight, $\bar{e}$ is the internal energy per unit mass, and c_v is the gas specific heat at constant volume. The following entropy representation of the equation of state is obtained by direct integration of the relation

$$t\,ds = de - p\,d\rho/\rho^2 \qquad (2.1.7)$$

after substitution of Eqs. (2.1.5) and (2.1.6):

$$\bar{s} - s_o = c_v \ln\left[(\bar{p}/p_o)(\rho_o/\bar{\rho})^{\gamma}\right] \qquad (2.1.8)$$

where

$$c_p = c_v + \mathcal{R}/(MW) \qquad (2.1.9)$$

and

$$\gamma = c_p/c_v \qquad (2.1.10)$$

where s is the entropy of the gas, c_p is the gas specific heat at constant pressure, and γ is the specific heat ratio of the gas.

Fluctuations are assumed to be small so that each quantity is only slightly perturbed. Hence, each quantity can be written as the sum of

an unperturbed or constant value designated by the subscript o and a small perturbation designated by the subscript 1:

$$\bar{\rho} = \rho_o + \rho_1 \tag{2.1.11}$$

$$\bar{u} = u_o + u_1 \tag{2.1.12}$$

$$\bar{u}_p = u_{p,o} + u_{p,1} \tag{2.1.13}$$

$$\bar{p} = p_o + p_1 \tag{2.1.14}$$

$$\bar{s} = s_o + s_1 \tag{2.1.15}$$

$$\bar{\phi} = \phi_o + \phi_1 \tag{2.1.16}$$

$$\bar{F} = F_o + F_1 \tag{2.1.17}$$

Substituting Eqs. (2.1.11) to (2.1.17) into Eqs. (2.1.1), (2.1.4), and (2.1.8) yields the following first-order system of equations:

$$D\rho_1/D\theta + \rho_o \, \partial u_1/\partial x = n\phi_1 \tag{2.1.18}$$

$$\rho_o Du_1/D\theta + \partial p_1/\partial x = nF_1 + n\phi_1(u_{p,o} - u_o) + n\phi_o(u_{p,1} - u_1) \tag{2.1.19}$$

$$D(s_1/c_p)/D\theta = D(p_1/\gamma p_o)/D\theta - D(\rho_1/\rho_o)/D\theta \tag{2.1.20}$$

where $D/D\theta$ is the substantial derivative, $D/D\theta = \partial/\partial\theta + u_o \partial/\partial x$.

Equation (2.1.20) is substituted into Eq. (2.1.18) to remove the density as a variable. The resulting equation in terms of non-dimensional parameters is

$$D(p_1/\gamma p_o)/D\theta + c_o \, \partial(u_1/c_o)/\partial x = n\phi_1/\rho_o + D(s_1/c_p)/D\theta \tag{2.1.21}$$

where c_o is the isentropic speed of sound given by

$$c_o^2 = \gamma \mathcal{R} t_o/(MW) = \gamma p_o/\rho_o \qquad (2.1.22)$$

Equation (2.1.19) can be written in terms of nondimensional parameters as

$$D(u_1/c_o)/D\theta + c_o\, \partial(p_1/\gamma p_o)/\partial x = nF_1/\rho_o c_o + (n\phi_1/\rho_o c_o)(u_{p,o} - u_o)$$

$$+ (n\phi_o/\rho_o c_o)(u_{p,1} - u_1) \qquad (2.1.23)$$

The wave equation discussed in this chapter is derived by making the following additional assumptions:

(1) The average mass production is zero.

$$\phi_o = 0 \qquad (2.1.24)$$

(2) The mean particle and gas velocity are both zero.

$$u_{p,o} = u_o = 0 \qquad (2.1.25)$$

Consequently, the one-dimensional, mixture, linearized conservation equations for zero mean flow relating perturbations in velocity, pressure, and density are as follows:

$$\partial(p_1/\gamma p_o)/\partial\theta + c_o\, \partial(u_1/c_o)/\partial x = n\phi_1/\rho_o + \partial(s_1/c_p)/\partial\theta \qquad (2.1.26)$$

$$\partial(u_1/c_o)/\partial\theta + c_o\, \partial(p_1/\gamma p_o)/\partial x = nF_1/\rho_o c_o \qquad (2.1.27)$$

A wave equation solution to these equations is found next.

The conservation Eqs. (2.1.26) and (2.1.27) contain unknown source terms ϕ_1, s_1, and F_1. In order to solve Eqs. (2.1.26) and (2.1.27), first, a small perturbation in pressure is assumed to cause a small perturbation in each source term. Consequently, transfer functions

$\mathcal{M}(\omega)/\rho_o$, $\mathcal{S}(\omega)/c_p$, and $\mathcal{F}(\omega)/\rho_o c_o$ relating a small change in mass, entropy, and drag force can be defined as follows:

$$\phi\left[n\phi_1/\rho_o\right] = (\mathcal{M}(\omega)/\rho_o)\phi\left[p_1/\gamma p_o\right] \tag{2.1.28}$$

$$\phi\left[s_1/c_p\right] = (\mathcal{S}(\omega)/c_p)\phi\left[p_1/\gamma p_o\right] \tag{2.1.29}$$

$$\phi\left[n\mathcal{F}_1/\rho_o c_o\right] = (\mathcal{F}(\omega)/\rho_o c_o)\phi\left[p_1/\gamma p_o\right] \tag{2.1.30}$$

where $\phi[\ ]$ is the Fourier transform operator and ω is the angular frequency.

The next step is to take the time and space Fourier transform of Eqs. (2.1.26) and (2.1.27) to obtain an algebraic equation. All perturbations are assumed to be proportional to $\exp\left[(ik_o\Omega - i\omega\theta)\right]$. Consequently, the Fourier transform of a function g of the independent variables θ and x produces another function denoted G of independent variables ω and $k_o\Omega$ defined by

$$G(\omega,k_o\Omega) = \int_{-\infty}^{\infty} e^{i\omega\theta} \int_{-\infty}^{\infty} g(\theta,x)e^{-ik_o\Omega x}\, dx\, d\theta = \phi\left[g(\theta,x)\right] \tag{2.3.31}$$

The inverse Fourier transform of a function G of the independent variables ω and $k_o\Omega$ produce another function, g, of the independent variables θ and x defined by

$$g(\theta,x) = \left(\frac{1}{2\pi}\right)^2 \int_{-\infty}^{\infty} e^{-i\omega\theta} \int_{-\infty}^{\infty} G(\omega,k_o\Omega)e^{ik_o\Omega x}\, d(k_o\Omega)d\omega = \phi^{-1}\left[G(\omega,k_o\Omega)\right] \tag{2.1.32}$$

To find the Fourier transform of a time derivative, the time derivative of Eq. (2.1.32) is taken

$$\partial g(\theta,x)/\partial\theta = (-i\omega)\phi^{-1}\left[G(\omega,k_o\Omega)\right] \tag{2.1.33}$$

Since the Fourier transform operation is unique, taking the Fourier transform of Eq. (2.1.33) yields

$$\phi\left[\partial g(\theta,x)/\partial\theta\right] = (-i\omega)\phi\left[g(\theta,x)\right] \tag{2.1.34}$$

The corresponding Fourier transform of a space derivative is

$$\phi\left[\partial g(\theta,x)/\partial x\right] = (ik_o\Omega)\phi\left[g(\theta,x)\right] \tag{2.1.35}$$

Taking the time and space Fourier transform of Eqs. (2.1.26) and (2.1.27) and substituting Eqs. (2.1.28) to (2.1.30) yields the following equation in matrix form

$$\begin{bmatrix} \left\{(-i\omega) - \left[\frac{\mathcal{M}(\omega)}{\rho_o} + (-i\omega)\,\frac{\mathcal{S}(\omega)}{c_p}\right]\right\} & c_o(ik_o\Omega) \\ \left[c_o(ik_o\Omega) - \frac{\mathcal{F}(\omega)}{\rho_o c_o}\right] & (-i\omega) \end{bmatrix} \phi\left[\begin{pmatrix} p_1/\gamma p_o \\ u_1/c_o \end{pmatrix}\right] = 0 \tag{2.1.36}$$

A non-trivial solution exists providing the determinant of the coefficient matrix vanishes. Solving the determinant yields a second-order polynomial equation for $(ik_o\Omega)$

$$\left(\frac{-i\omega}{c_o}\right)\left\{\left(\frac{-i\omega}{c_o}\right)-\left[\frac{\mathcal{A}(\omega)}{\rho_o c_o}+\left(\frac{-i\omega}{c_o}\right)\frac{\mathcal{B}(\omega)}{c_p}\right]\right\}-(ik_o\Omega)\left[(ik_o\Omega)-\frac{\mathcal{F}(\omega)}{\rho_o c_o^2}\right]=0 \tag{2.1.37}$$

The solution to Eq. (2.1.37) is given by

$$(ik_o\Omega)=\frac{1}{2}\left\{\frac{\mathcal{F}(\omega)}{\rho_o c_o^2}\pm\left(\left[\frac{\mathcal{F}(\omega)}{\rho_o c_o^2}\right]^2+4\beta\right)^{1/2}\right\} \tag{2.1.38}$$

where

$$\beta=\left(\frac{-i\omega}{c_o}\right)^2\left\{1-\left(\frac{-i\omega}{c_o}\right)^{-1}\left[\frac{\mathcal{A}(\omega)}{\rho_o c_o}+\left(\frac{-i\omega}{c_o}\right)\frac{\mathcal{B}(\omega)}{c_p}\right]\right\} \tag{2.1.39}$$

An approximate solution to the wave number equation (Eq. (2.1.37)) is given by Marble and Candel (1975). This solution may be obtained from the exact solution (Eq. (2.1.38)) by assuming that

$$\left|\frac{\mathcal{F}(\omega)}{\rho_o c_o^2}\right|^2 \ll 4\beta \tag{2.1.40}$$

and that

$$\left|\left(\frac{-i\omega}{c_o}\right)^{-1}\left[\left(\frac{\mathcal{A}(\omega)}{\rho_o c_o}\right)+\left(\frac{-i\omega}{c_o}\right)\frac{\mathcal{B}(\omega)}{c_p}\right]\right| \ll 1 \tag{2.1.41}$$

With these assumptions and after some algebraic manipulation the two approximate wave number solutions to Eq. (2.1.37) are

$$(ik_o\Omega)^+ = i\left\{\left(\frac{\omega}{c_o}\right)-\left(\frac{i}{2c_o}\right)\left[\frac{\mathcal{M}(\omega)}{\rho_o} + (-i\omega)\,\frac{\mathcal{S}(\omega)}{c_p} + \frac{\mathcal{F}(\omega)}{\rho_o c_o}\right]\right\} \qquad (2.1.42)$$

$$(ik_o\Omega)^- = -i\left\{\left(\frac{\omega}{c_o}\right)-\left(\frac{i}{2c_o}\right)\left[\frac{\mathcal{M}(\omega)}{\rho_o} + (-i\omega)\,\frac{\mathcal{S}(\omega)}{c_p} - \frac{\mathcal{F}(\omega)}{\rho_o c_o}\right]\right\} \qquad (2.1.43)$$

The wave number for waves moving to the right used by Marble and Candel (1975) is given by Eq. (2.1.42) in terms of the notation used herein.

By definition, the sound propagation velocity is related to the wave number equation by

$$c(\omega) = \frac{\omega}{\mathrm{Im}(ik_o\Omega)},\ \mathrm{m/sec} \qquad (2.1.44)$$

Also by definition, the acoustic energy attenuation coefficient in Nepers per meter is

$$\alpha = -2\ \mathrm{Re}(ik_o\Omega) \qquad (2.1.45)$$

Nepers per meter is converted to decibels per meter by multiplying by 10 log e = 4.34:

$$\alpha = -8.68\ \mathrm{Re}(ik_o\Omega),\ \mathrm{dB/m} \qquad (2.1.46)$$

In this section the fundamental governing equations were discussed. Furthermore, for the case where the average mass production, mean particle velocity, and mean gas velocity are zero, equations for calculating the sound propagation speed and the attenuation of a plane pressure wave propagating in a cloud of particles were determined. These equations depend on transfer functions relating a small change in mass production, entropy production, and drag force to a small change in pressure. The

derivation of these transfer functions for the case of a plane wave propagating in a cloud of liquid fuel drops and a cloud of solid soot particles is discussed next.

B. Response of the Fuel Droplet Cloud

Fuel droplet emissions from combustors in the combustion duct system can occur when the fuel droplet spray consists of large-diameter drops and the air injected around the fuel nozzle through swirlers mi es poorly with the fuel spray. This combination of large fuel drops and poor mixing produces high levels of hydrocarbon emission (Jones (1977)). The larger droplets which pass through the high temperature reaction zone are assumed to evaporate in a relatively cool gas mixture having a low oxygen concentration. Accordingly, the process is approximated by considering evaporation without combustion (Faeth (1977)).

The processes and assumptions typically employed in an analysis of fuel drop evaporation are discussed by Graves and Bahr (1950), Faeth (1977), and Harrje (1972). However, rather than using a complex model to obtain expressions for $\mathcal{M}(\omega)/\rho_o$, $\mathcal{J}(\omega)/c_p$, and $\mathcal{F}(\omega)/\rho_o c_o$, the approximate model used by Marble and Candel (1975) for water drop evaporation is adapted for use herein by making appropriate assumptions. This model is discussed in Appendix A. The resulting expressions provide: (1) a guide to the order of magnitude of the transfer functions $\mathcal{M}(\omega)/\rho_o$, $\mathcal{J}(\omega)/c_p$, and $\mathcal{F}(\omega)/\rho_o c_o$, and (2) information on the frequency dependence of the sound propagation speed and the attenuation. Because the resulting expressions are identical to those which could be obtained from expressions derived by Marble and Candel (1975), they are shown in Appendix A. The numerical values of the factors in these expressions are different because the physical properties were changed

to those for a fuel drop rather than those for a water drop. The results of calculations using this theory are discussed in section D.

C. Response of the Soot Particle Cloud

Soot produced by gas turbine combustors oxidizes as it flows through the duct system (Linden and Heywood (1971), Norgren (1971), and Gouldin (1973)). In order to accurately calculate the response of a cloud of soot particles to an acoustic pressure perturbation, the mass distribution, the chemical composition, and the distribution of particle shapes and sizes should be known. It is also necessary to know the rate constants for the heterogenous oxidation process and the heat transfer process. However, at this time none of this information is known accurately. Consequently, the following model includes the basic physics and chemistry in only an approximate manner. An experimental study of the oxidation of soot by Wright (1975) and a mathematical model for the gasification of coal char discussed by Simmons and Lewis (1977) were useful in formulating the approach used in this work. The model is based on the assumption that the soot particles can be treated as being made of porous carbon, having a spherical shape, and having a uniform temperature.

The transfer functions $\mathcal{M}(\omega)/\rho_o$, $\mathcal{J}(\omega)/c_p$, and $\mathcal{F}(\omega)/\rho_o c_o$ are derived from equations that describe the particulate phase of the one-dimensional flow of the gas-soot particle mixture with transfer of mass, momentum, and energy. When specifying the functional dependence of $\mathcal{F}(\omega)/\rho_o c_o$ and $\mathcal{J}(\omega)/c_p$, the following selection is made. As previously discussed, for the force acting on the gas due to a particle, Stokes' viscous drag law is used. Thus, the total force on the gas is

$$\bar{F} = -n6\pi r_s \mu(\bar{u} - \bar{u}_s) \qquad (2.3.1)$$

For the heat transfer from the particles to the gas, Newton's law of convection is used. Thus, the total heat transfer from n soot particles into a unit volume of gas having thermal conductivity k is

$$\bar{Q} = n\left(4\pi r_s^2\right)\left(\frac{Nu_H}{d_s}\right)\kappa(\bar{t}_s - \bar{t}_\infty) \tag{2.3.2}$$

where the heat-transfer Nusselt number Nu_H equals 2 if the air is stagnant. The value 2 which is generally assumed, is used herein since the difference between the particle velocity and the gas velocity is assumed small.

The viscous drag transfer function is discussed first. A soot particle of mass m_s and radius r_s is moving with a velocity $u_{s,1}$ in the gas. The gas has a velocity u_1 due to the wave motion. The particle experiences a Stokes' drag force of $6\pi r_s\mu(u_1 - u_{s,1})$, and the resulting particle equation of motion is

$$m_s \frac{du_{s,1}}{d\theta} = F_1 = 6\pi r_s\mu(u_1 - u_{s,1}) \tag{2.3.3}$$

The gas velocity is related to a pressure perturbation for small perturbations by

$$u_1 = c_o p_1/\gamma p_o \tag{2.3.4}$$

The time Fourier transform of Eq. (2.3.3) yields the following expression for the response of the particle velocity to a pressure perturbation:

$$\Phi\left[u_{s,1}\right] = \frac{c_o}{1 + (-i\omega)\tau}\,\Phi\left[\frac{p_1}{\gamma p_o}\right] \tag{2.3.5}$$

where

$$\tau = \frac{m_s}{6\pi r_s \mu} \tag{2.3.6}$$

Physically, the time constant τ is the time interval in which the particle velocity is reduced by a factor of $1/e$ from its initial value due to the Stokes' drag force. Substituting Eqs. (2.3.4) and (2.3.5) into Eq. (2.3.3) and using Eq. (2.1.30) yields the following expression for the viscous drag force perturbation in response to a pressure perturbation:

$$\Phi\left[\frac{F_1}{\rho_o c_o}\right] = -\frac{n6\pi r_s \mu}{\rho_o c_o}\left[\frac{c_o(-i\omega)\tau}{1 + (-i\omega)\tau}\right]\Phi\left[\frac{p_1}{\gamma p_o}\right] \tag{2.3.7}$$

Consequently, the viscous drag force transfer function is given by

$$\frac{\mathcal{F}(\omega)}{\rho_o c_o} = -\frac{\kappa_s}{\tau}\left[\frac{(-i\omega)\tau}{1 + (-i\omega)\tau}\right] \tag{2.3.8}$$

where

$$\kappa_s = \frac{nm_s}{\rho_o} \tag{2.3.9}$$

The heat generated by the oxidation of a soot particle is assumed to be transferred directly to the particle. Thus, the entropy source perturbation term may be calculated considering only the heat transfer between the n particles and the bulk gas using Eq. (2.3.2) as follows:

$$t_o \rho_o \frac{ds_1}{d\theta} = Q_1 = n\left(4\pi r_s^2\right)\frac{Nu_H}{d_s}\kappa(t_{s,1} - t_{\infty,1}) \tag{2.3.10}$$

The differential equation for the entropy source perturbation can then be written

$$\frac{d}{d\theta}\left(\frac{s_1}{c_p}\right) = \frac{\kappa_s}{\tau_s}\left(\frac{t_{s,1} - t_{\infty,1}}{t_o}\right) \qquad (2.3.11)$$

where

$$\tau_s = \frac{m_s c_p}{4\pi r_s^2 \left(\frac{Nu_H}{d_s}\right)\kappa} \qquad (2.3.12)$$

Physically, the time constant τ_s is the time interval in which the gas entropy is changed by a factor of $1/e$ from its initial value.

Perturbations in bulk gas temperature and pressure are related to perturbations in soot particle temperature by combining the time derivative of the bulk gas energy equation (Eq. (2.1.20) with $u_o = 0.0$) with the perfect gas law and Eq. (2.3.11) to show

$$\frac{d}{d\theta}\left(\frac{t_{\infty,1}}{t_o}\right) - (\gamma - 1)\frac{d}{d\theta}\left(\frac{p_1}{\gamma p_o}\right) = \frac{\kappa_s}{\tau_s}\left(\frac{t_{s,1} - t_{\infty,1}}{t_o}\right) \qquad (2.3.13)$$

The slowest process in the burning of a soot particle controls the reaction rate. Depending on the temperature and the particle geometry, this may either be the diffusion of oxygen to the particle surface or the chemical reaction rate at the surface. For this model, the chemical reaction rate is assumed to be slower than the diffusion rate (Linden and Heywood (1971)). Consequently, it controls the oxidation process. The soot is, for simplicity, assumed to be carbon. However, evidence exists that the soot contains a few percent hydrogen which, in practice, could be important. To model the chemical reaction of

oxygen with the soot, an adsorption/desorption mechanism is used involving the following sequence of reactions:

$$C + O_2 \xrightarrow{K_1} (CO_2)_a$$

$$(CO_2)_a \xrightarrow{K_2} C + O_2$$

$$C + (CO_2)_a \xrightarrow{K_3} 2CO$$

where $(CO_2)_a$ is a surface oxide (i.e., an O_2 molecule adsorbed on the carbon surfaces (Wright (1975), Simmons and Lewis (1977)).

This process may be followed by a gasification reaction which produces carbon dioxide (Wright (1975)). Only the initial production of carbon monoxide is considered herein.

The following concentration equations can be written for the sequence of chemical reactions considered:

$$\frac{d}{d\theta}\left[(CO_2)_a\right] = K_1[O_2] - K_2\left[(CO_2)_a\right] - K_3\left[(CO_2)_a\right] \qquad (2.3.14)$$

$$-\frac{d}{d\theta}[C] = -K_2\left[(CO_2)_a\right] + K_1[O_2] \qquad (2.3.15)$$

The concentration of $(CO_2)_a$ is assumed constant because a steady-state condition is achieved where as much is created as is destroyed. Consequently, the time derivative of $(CO_2)_a$ is zero. Thus, the left side of Eq. (2.3.14) can be set to zero, and the following expression for the concentration of $(CO_2)_a$ is obtained:

$$\left[(\omega_2)_a\right] = \frac{K_1\left[O_2\right]}{K_2 + K_3} \tag{2.3.16}$$

The carbon consumption rate, which equals the net rate at which mass is added to the gas by a single particle per unit particle surface area, is then given by

$$\frac{d}{d\theta}\left[C\right] = K_1\left[O_2\right] - \frac{K_2K_1\left[O_2\right]}{K_2 + K_3} = \frac{K_1K_3}{K_2 + K_3}\frac{p_{O_2}}{\mathcal{R}t} \tag{2.3.17}$$

$$= K_a p_{O_2}$$

The following Arrhenius model chemical reaction rates (from Simons and Lewis (1977)) were determined empirically to fit a wide range of data:

$$K_3 = 9500\, e^{-19,700/t} \text{ kg/m}^2\text{-sec} \tag{2.3.18}$$

$$K_1/\mathcal{R}t = 2\times10^{-2}\, e^{-15,700/t} \text{ kg/N-sec} \tag{2.3.19}$$

$$K_2 = 5.5\, 10^7\, e^{-38,700/t} \text{ kg/m}^2\text{-sec} \tag{2.3.20}$$

The rate of mass addition to the bulk gas per unit volume for soot particles having surface area a_s is then

$$n\phi = na_sK_ap_{O_2} \tag{2.3.21}$$

For a small perturbation in surface temperature and oxygen particle pressure, the resulting change in mass addition can be written as

$$n\bar{\phi} = n\phi_o + n\phi_1 = na_sK_a\left[1 + \frac{t_o}{K_a}\frac{dK_a}{dt}\frac{t_{s,1}}{t_o}\right]p_{O_2,o}\left[1 + \frac{p_{O_2,1}}{p_{O_2,o}}\right] \tag{2.3.22}$$

Thus, the mass perturbation term is given by

$$n\phi_1 = (n a_s K_a p_o)\left(\frac{p_{O_{2,o}}}{p_o}\right)\left[\left(\frac{t_o}{K_a}\frac{dK_a}{dt}\right)\frac{t_{s,1}}{t_o} + \frac{p_{O_{2,1}}}{p_{O_{2,o}}}\right] \qquad (2.3.23)$$

This equation is rewritten as

$$\frac{n\phi_1}{\rho_o} = \frac{\kappa_s}{\tau_a} Y_{O_2} \zeta \frac{t_{s,1}}{t_o} + \frac{\kappa_s}{\tau_a} Y_{O_2} \frac{p_{O_{2,1}}}{p_{O_{2,o}}} \qquad (2.3.24)$$

where

$$\tau_a = \frac{1}{A_I K_a p_o} \qquad (2.3.25)$$

$$A_I = \frac{a_s}{m_s} \qquad (2.3.26)$$

$$Y_{O_2} = \frac{p_{O_{2,o}}}{p_o} \qquad (2.3.27)$$

and

$$\zeta = \frac{t_o}{K_a}\frac{dK_d}{dt} \qquad (2.3.28)$$

The external surface area per unit mass of a spherical carbon particle of diameter d_s is

$$A_E = \frac{4\pi r_s^2}{m_s} = 4\pi\left(\frac{d}{2}\right)^2 \frac{1}{\frac{4}{3}\pi\left(\frac{d}{2}\right)^3 2000}\frac{m^2}{kg} \quad \frac{3}{1000\, d_s}\frac{m^2}{kg} \qquad (2.3.29)$$

Typical internal surface area per unit mass of coal char as measured by molecular adsorption are 100,000 to 400,000 m^2/kg for 100 μ particles

which is four orders of magnitude greater than the external surface area per unit mass (Simmons and Lewis (1977)). Consequently, the model calculations made herein use internal surface areas per unit mass approximately four orders of magnitude greater than the external surface areas per unit mass.

The oxidation reaction is

$$C + \frac{1}{2} O_2 \rightarrow CO$$

The heat generated is given by

$$Q_c = \left(\sum_P n_l h_l - \sum_R n_e h_e \right) \frac{1}{(MW)_C} \qquad (2.3.30)$$

The heat balance equation for a soot particle is then

$$\frac{d}{d\theta} (m_s c_s t_{s,l}) = -\left(4\pi r_s^2\right) \left(\frac{Nu_H}{d_s} \right) \kappa (t_{s,l} - t_{\infty,l}) - Q_c \phi_l \qquad (2.3.31)$$

When all n particles are considered, Eq. (2.3.31) becomes

$$\kappa_s \frac{c_s}{c_p} \frac{d}{d\theta} \left(\frac{t_{s,l}}{t_o} \right) = - \frac{\kappa_s}{\tau_s} \left(\frac{t_{s,l} - t_{\infty,l}}{t_o} \right) - \varepsilon \frac{n\phi_l}{\rho_o} \qquad (2.3.32)$$

where

$$\varepsilon = \frac{Q_c}{t_o c_p} \qquad (2.3.33)$$

The perturbation in the partial pressure of oxygen is related to the mass source variation and the total pressure perturbation using the continuity equations. The oxygen continuity equation is

$$\frac{\partial}{\partial\theta}\rho_{O_{2,1}} + \rho_{O_{2,o}}\frac{\partial u_1}{\partial x} = -n\phi_1\frac{16}{12} \tag{2.3.34}$$

for when a mass of carbon, ϕ_1, is added to the gas the oxygen concentration is reduced by 16 ϕ/12. The bulk gas continuity equation is

$$\frac{\partial}{\partial\theta}\rho_1 + \rho_o\frac{\partial}{\partial x} = n\phi_1 \tag{2.3.35}$$

The velocity gradient is eliminated from Eqs. (2.3.34) and (2.3.35) as follows:

$$\frac{\partial u_1}{\partial x} = \frac{n\phi_1}{\rho_o} - \frac{1}{\rho_o}\frac{\partial\rho_1}{\partial\theta} = \frac{-\frac{16}{12}n\phi_1}{\rho_{O_{2,o}}} - \frac{1}{\rho_{O_{2,o}}}\frac{\partial\rho_{O_{2,1}}}{\partial\theta} \tag{2.3.36}$$

Thus,

$$\frac{n\phi_1}{\rho_o}\left(1 + \frac{\rho_o}{\frac{12}{16}\rho_{O_{2,o}}}\right) = \frac{1}{\rho_o}\frac{\partial\rho_1}{\partial\theta} - \frac{1}{\rho_{O_{2,o}}}\frac{\partial\rho_{O_{2,1}}}{\partial\theta} \tag{2.3.37}$$

However, the oxygen and the bulk gas temperature are identical, and the gas properties are assumed to be identical; that is, both behave as perfect gases. Consequently, Eq. (2.3.37) can be written in terms of pressure perturbations as follows:

$$\frac{n\phi_1}{\rho_o}\left(\frac{1 + \frac{12}{16}Y_{C_2}}{\frac{12}{16}Y_{O_2}}\right) = \frac{\partial}{\partial\theta}\left(\frac{p_1}{p_o} - \frac{p_{O_{2,1}}}{p_{O_{2,o}}}\right) \tag{2.3.38}$$

Equation (2.3.24) and the Fourier transforms of Eqs. (2.3.13), (2.3.32), and (2.3.38) can be put in the following matrix form:

$$\mathcal{A}\vec{Y} = \begin{bmatrix} 0 & -\frac{\kappa_s Y_{O_2}\zeta}{\tau_a} & 1 & \frac{\kappa_s Y_{O_2}}{\tau_a} \\ \left[(-i\omega) + \frac{\kappa_s}{\tau_s}\right] & -\frac{\kappa_s}{\tau_s} & 0 & 0 \\ -\frac{\kappa_s}{\tau_s} & \left[\frac{\kappa_s c_s(-i\omega)}{c_p} + \frac{\kappa_s}{\tau_s}\right] & \varepsilon & 0 \\ 0 & 0 & \frac{1}{\gamma}\left[\frac{Y_{O_2}\frac{12}{16} + 1}{Y_{O_2}\frac{12}{16}}\right] & \left(\frac{-i\omega}{\gamma}\right) \end{bmatrix} \Phi \begin{bmatrix} \frac{t_{\infty,1}}{t_o} \\ \frac{t_{s,1}}{t_o} \\ \frac{n\phi_1}{\rho_o} \\ \frac{p_{O_{2,1}}}{p_{O_{2,o}}} \end{bmatrix} = \begin{bmatrix} 0 \\ (-i\omega)(\gamma - 1) \\ 0 \\ (-i\omega) \end{bmatrix} \Phi\left[\frac{p}{\gamma p_o}\right] = \vec{U} \qquad (2.3.39)$$

The solution is

$$\vec{Y} = \mathcal{M}^{-1}\vec{U} \tag{2.3.40}$$

The mass source transfer function is found by using the solution for ϕ_1/ρ_0 obtained from Eqs. (2.3.39) and (2.1.28). The entropy source transfer function is found using the quantities $\phi[t_{s,1}/t_o]$ and $\phi[t_{\infty,1}/t_o]$ which were obtained from Eq. (2.3.39), the Fourier transform of Eqs. (2.3.11) and (2.1.29).

In this section the response of a soot particle cloud to a pressure perturbation was investigated. As a result equations were derived for calculating the transfer functions relating a small change in mass production, entropy production, and drag force to a small change in pressure. The next section discusses typical dispersion and attenuation curves calculated for sound propagation in a liquid fuel droplet cloud and in a soot particle cloud.

D. Sample Calculations

A typical dispersion curve and an attenuation curve calculated for vaporizing fuel droplets by using the arbitrary parameters in Table I are presented in Figure 2. The propagation velocity varies from 506 m/sec at low frequencies to the isentropic speed of sound (610 m/sec) at high frequencies. The attenuation is greater than 3 dB/m above 400 Hz.

The relative importance of the transfer functions $\mathcal{M}(\omega)/\rho_o$, $\mathcal{S}(\omega)/c_p$, and $\mathcal{F}(\omega)/\rho_o c_p$ in calculating attenuation and dispersion using Eqs. (2.1.42), (2.1.44), and (2.1.46) can be determined from Figure 3. The viscous drag transfer function, $\mathcal{F}(\omega)/\rho_o c_o$, and the mass source transfer function, $\mathcal{M}(\omega)/\rho_o$, shown in Figure 3 have negligible effects at combustion noise frequencies which are below 500 Hz. Consequently, the entropy source transfer function determines the attenuation

TABLE I. - Parameters[a] used to calculate dispersion and attenuation for the case of fuel droplets vaporizing

t, K 922.0	κ_v 0.05
κ, W/m-k . . . . . $5.38/100^{-2}$	H_{VL}, J/kg . . . . . 4.16×10^{7}
ρ_o, kg/m^3 . . . . . 0.378	nm_L, kg/m^3 . . . . . 0.0058
c_p, J/kg-K 1100.0	c_o, m/sec 610.0
γ 1.4	η, $H_{VT}/T_o c_p$ 41
ρ_L, kg/m^3 . . . . . 845.0	β, $(MW)_v/(MW)_g$ 3.94
c_L, J/kg-K 1700	n . . . . . 1.64×10^{13}
r_L, m . . . . . 1100×10^{-6}	m_L, kg . . . . . 3.54×10^{-15}
$(MW)_g$ 28.97	κ_L, NM_L/ρ_o . . . . . 1.53×10^{-2}
$(MW)_L$ 114.0	τ, sec . . . . . 5.13×10^{-6}
μ, kg/m-sec . . . . 3.66×10^{-5}	τ_D, sec . . . . . 1.64×10^{-5}
D_{Vg}, m^2/sec . . . . 4.54×10^{-5}	τ_{TL}, sec . . . . . 1.18×10^{-5}

[a]Defined in Appendix A.

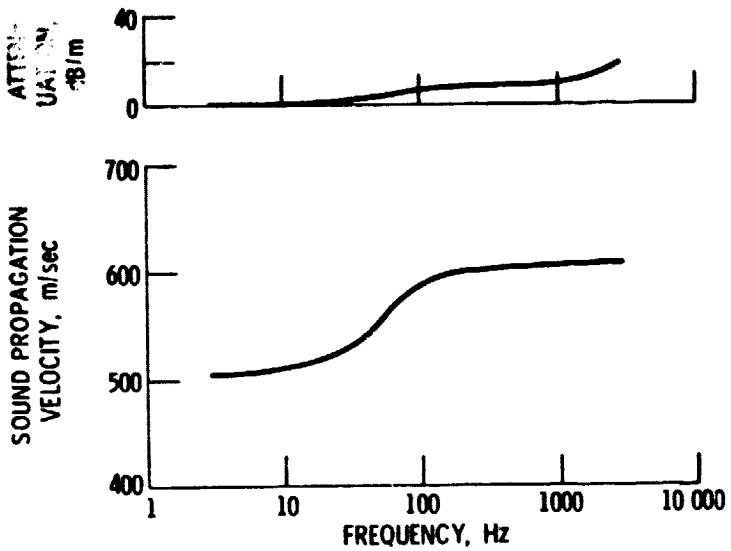

Figure 2. - Calculated acoustic attenuation and dispersion in region containing vaporizing fuel droplets.

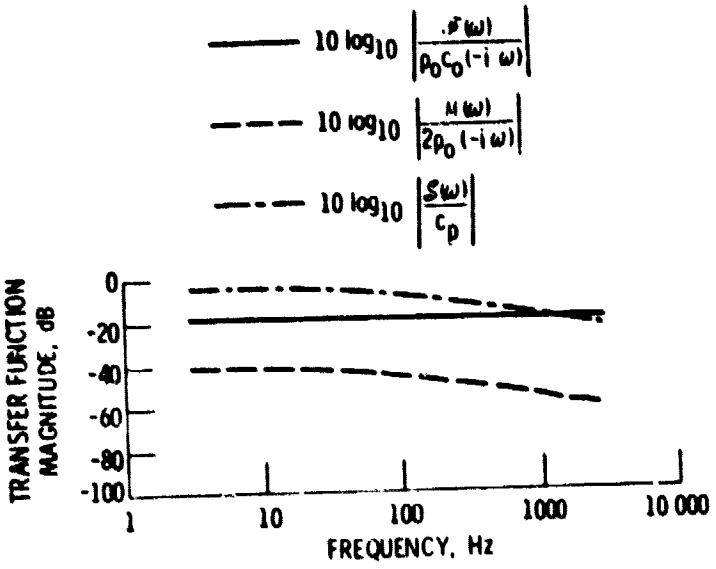

Figure 3. - Calculated viscous drag force, mass source and entropy source transfer functions in a region containing vaporizing fuel droplets.

and dispersion at low frequencies. Specifically, the viscous drag force transfer function can be neglected below 1200 Hz. Above 1200 Hz the entropy transfer function becomes less than the viscous drag force transfer function and this accounts for the increase in the attenuation shown in Figure 2 above 1200 Hz.

A typical dispersion curve and an attenuation curve calculated for oxidizing soot particles by using the arbitrary parameters in Table II are shown in Figure 4. for soot particle mass fractions of 0.015 (example 1, Table II) and 0.0014 kg/m^3 (example 2, Table II) and an oxygen partial pressure of 0.05. The sound propagation speed varies from 440 m/sec for a mass fraction of 0.0014 and from 420 m/sec for a mass fraction of 0.015 at low frequencies to the isentropic speed of sound (610 m/sec) at high frequencies. The attenuation for a mass fraction of 0.015 is greater than 3 dB/m above 400 Hz. However, it drops to less than 1 dB/m for a mass fraction of 0.0014. It was also found that for these cases the viscous drag force transfer function and the mass source transfer function could be neglected at low frequencies.

In this chapter the propagation of a plane wave through a stationary gas containing a particle cloud of either liquid fuel droplets or solid soot particles was studied. The fundamental governing equations were discussed. In addition, sample calculations were made producing typical dispersion and attenuation curves for both cases. Sample transfer function calculations for the liquid fuel droplet cloud case were also presented. The failure of the use of the isentropic sound propagation speed to predict the frequencies of longitudinal duct resonance modes is explained as being due to the presence of clouds of particles which cause the sound to propagate at a lower velocity at combustion

TABLE II. - Parameters used to calculate dispersion and attenuations curves for the case of soot particles oxidizing

t_o, K 922.0	Q, J/kg . . . . . -3.637×10^{6}
κ, W/m-K . . . . . 5.38×10^{-2}	A_I, m^2/kg . . . . . 4.0×10^{8}
ρ, kg/m^3 . . . . . 0.378	c_o, m/sec 609.0
c_p, J/kg-K 1100.0	ε, $Q/T_o c_p$ . . . . . -3.585
γ 1.4	K_a, kg/N-sec . . . 8.08×10^{-10}
ρ_s, kg/m^3 . . . . . 1880.0	$\frac{T_o}{K_a}\frac{dK_a}{dT}$ 17.0
c_s, J/kg-m^3 . . . . . 3200.0	m_s, kg . . . . . 7.87×10^{-15}
r_s, m . . . . . 1.0×10^{-6}	τ, sec . . . . . 1.14×10^{-5}
$(MW)_g$ 28.97	τ_s, sec . . . . . 1.50×10^{-6}
μ, kg/m-sec . . . . 3.66×10^{-5}	τ_a, sec . . . . . 3.09×10^{-5}
κ_{O_2} 0.05	

	Example	
	1	2
n	7.36×10^{11}	6.73×10^{10}
nm_s, kg/m^3	5.8×10^{-3}	5.3×10^{-4}
κ_s, nm_s/ρ_o	1.5×10^{-2}	1.4×10^{-3}

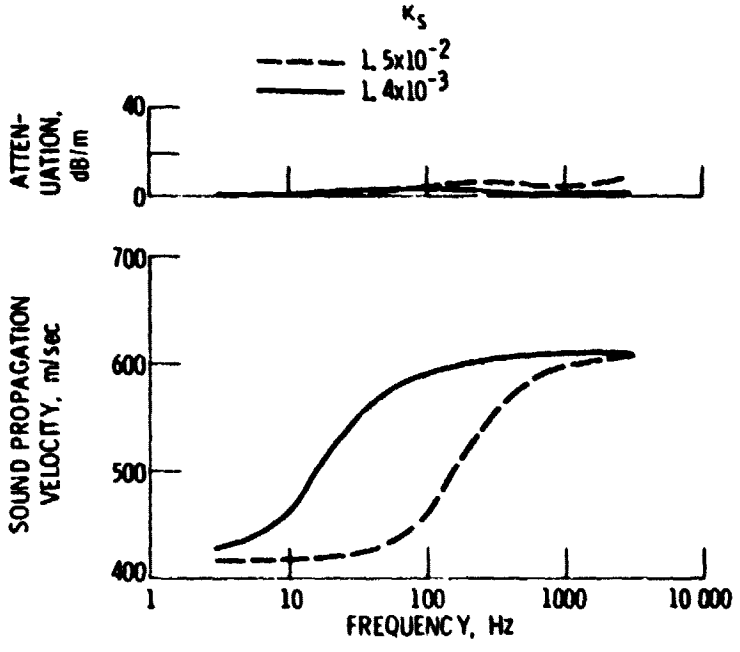

Figure 4. - Attenuation and dispersion for oxidizing soot particles.

noise frequencies. In the next chapter the propagation of a plane wave through a moving gas containing a soot particle cloud is discussed. Moreover, a model for the operating ducted combustor system will be described which can be used to calculate in-duct pressure auto-spectra and cross-spectra.

Symbols Used in This Chapter

$\mathcal{A}$	matrix
A_E	soot particle exterior area per unit mass, m^2/kg
A_I	soot particle interior area per unit mass, m^2/kg
a_s	soot particle surface area, m^2
c	soot mass, kg
$c(\omega)$	sound propagation speed, m/sec
c_o	isentropic speed of sound, m/sec
c_p	gas specific heat at constant pressure, J/kg-K
c_s	soot particle specific heat, J/kg-K
c_v	gas specific heat at constant volume, J/kg-K
d	diameter, m
e	internal energy, J/kg
F	particle force exerted on gas
$\mathcal{F}(\omega)/\rho_o c_o$	viscous drag transfer function
f	frequency, Hz
H	heat-transfer coefficient, W/m^2-K
i	$(-1)^{1/2}$
K_a	effective chemical reaction rate, kg-N-sec
K_ℓ	chemical reaction rate of the ℓ^{th} process
k_o	propagation wave number, ω/c_o, m^{-1}

$\mathcal{M}(\omega)/\rho_o$	mass source transfer function
(MW)	molecular weight
m	soot particle mass, kg
Nu_H	heat-transfer Nusselt number, Hd/κ
n	number of particles per unit volume
n_i, n_e	number of moles
p	pressure, N/m^2
p_{O_2}	partial pressure of oxygen, N/m^2
Q	heat transferred to gas from particles by convection
Q_c	heat generated by chemical reaction per unit mass of fuel, J/kg
$\mathcal{R}$	gas constant
r	particle radius, m
$\mathcal{S}(\omega)/c_p$	entropy source transfer function
s	entropy of gas, J/kg-K
t	temperature, K
$\vec{U}$	system forcing function
u	velocity, m/sec
x	Cartesian coordinate
$\vec{Y}$	system state vector
Y	relative concentration, partial pressure ratio or density ratio
α	acoustic attenuation coefficient, dB/m
β	see Eq. (2.1.39)
γ	specific heat ratio of gas
ϵ	chemical heat parameter, $Q_c/c_p t_o$
ζ	chemical reaction rate parameter, $(t_o/K_a)(dK_a/dt)$

θ	time, sec
κ	gas thermal conductivity, W/m-K
κ_s	soot particle mass fraction, nm_s/ρ_o
μ	gas dynamic viscosity, kg/m-sec
ρ	gas density, kg/m^3
τ	Stokes' relaxation time, $m/6\pi r_s \mu$, sec
τ_a	adsorption relaxation time, $1/A_I K_a p_o$, sec
τ_s	soot particle thermal relaxation time, $(m_s c_p)/4\pi r^2 (Nu_H/d_s)\kappa$, sec
$\phi[\ ]$	Fourier transform operator
ϕ	mass source rate
Ω	dispersion-attenuation propagation wave number factor
ω	angular frequency, $2\pi f$, radians/sec

Superscripts and subscripts:

$(\vec{\ })$	vector quantity
$(\bar{\ })$	instantaneous quantity
$(\ )^+$	downstream propagating
$(\ )^-$	upstream propagating
a	adsorbed
C	carbon
H	heat transfer
O_2	molecular oxygen
o	reference state
p	particle
s	soot
1	perturbed quantity
∞	in bulk gas far from soot particle

III. ACOUSTIC MODEL OF THE COMBUSTION DUCT SYSTEM

The effect of attenuation and dispersion on duct spectra measured in a flowing confined gas containing soot particles is discussed in this chapter. The analysis presented in the last chapter investigated attenuation and dispersion in a stationary, infinite bulk gas containing particles. Consequently, the previous analysis must be modified to take into account the presence of mean flow.

In the last chapter it was determined that the viscous drag transfer function $\mathcal{F}(\omega)/\rho_o c_o$, and the mass source transfer function, $\mathcal{M}(\omega)/\rho_o$, have negligible effects at combustion noise frequencies on attenuation and dispersion. Thus, the entropy source transfer function, $\mathcal{J}(\omega)/c_p$, determines the attenuation and dispersion at low frequencies. However, the entropy source transfer function, $\mathcal{J}(\omega)/c_p$, defined in Chapter I depends on terms related to the mass source.

In this chapter, it is assumed at the start that the viscous drag transfer function, $\mathcal{F}(\omega)/\rho_o c_o$, and the mass transfer function, $\mathcal{M}(\omega)/\rho_o$, have negligible effect at combustion noise frequencies on attenuation and dispersion and that only the entropy source transfer function, $\mathcal{J}(\omega)/c_p$, is important.

In addition, the entropy source transfer function, $\mathcal{J}(\omega)/c_p$, defined in this chapter will be determined by assuming that the consequences of soot particle surface oxidation can be idealized as producing a constant time-independent soot particle temperature. Consequently, the model presented in this chapter includes only the effect of

heat transfer between the soot particles and the flowing gas. This assumption yields a set of equations dependent on only a single time constant. As a consequence, the equations can be formulated as a distributed system parameter identification problem with a single unknown time constant. The model described in Chapter I is more complex and depends on more parameters.

An extensive review of the distributed system parameter identification problem is given by Polis and Goodsen (1976). Rather than using any of the methods described by Polis and Goodsen to evaluate the unknown time constant, it will be evaluated as follows. First, the solution to the problem discussed herein is approximated by the solution to an acoustic wave equation. Then, the acoustic wave equation and its solution are used to model the propagation in the duct system and to calculate auto-spectra and cross-spectra. Finally, by comparing measured spectra and calculated spectra the unknown time constant may be determined.

A. Analysis

1. Model Wave Equation

The mass transfer and the body force due to viscous drag are neglected. Consequently, Eqs. (2.1.18) and (2.1.19) yield in non-dimensional form the following one-dimensional continuity and momentum equations relating small perturbations:

$$D(\rho_1/\rho_o)/D\theta + c_o \partial(u_1/c_o)/\partial x = 0 \qquad (3.1.1)$$

$$D(u_1/c_o)/D\theta + c_o \partial(p_1/\gamma p_o)/\partial x = 0 \qquad (3.1.2)$$

The energy equation derived by considering only the heat transfer between the particles and the bulk gas is

$$\overline{t\rho}\,\overline{Ds}/D\theta = n\dot{\overline{Q}} \tag{3.1.3}$$

where the heat transfer rate per soot particle from the particle into a unit volume of gas is

$$\dot{\overline{Q}} = \left(4\pi r_s^2\right)(Nu_H/d_s)\kappa(\overline{t}_s - \overline{t}_\infty) \tag{3.1.4}$$

This equation is similar to Eq. (2.3.10). However, the total derivative appears in place of the time derivative since the gas has a mean velocity. The total derivative is given by

$$D/D\theta = \partial/\partial\theta + u_o\partial/\partial x$$

where the first term on the right side is the temporal member and the second term is the convective member in the x direction. When the mean flow is zero, as it was assumed to be in the previous chapter, the convective member is zero. However, even with flow, when the entropy is constant the convective term is frequently neglected if the time to convect a disturbance through the volume of interest is large compared with the time required for a quantity to change from a minimum to a maximum. The entropy is not constant in this problem since the heat transfer between the soot particles and gas is taken into account. Therefore, the effect on the attenuation and dispersion of the convective term and the heat transfer term may be of the same order of magnitude. Consequently, the convective term is included in the governing equations.

In deriving the small perturbation form of the energy equation the soot particle temperature is assumed to be time-independent

$$t_s = t_{s,o} \tag{3.1.5}$$

Consequently, for small perturbations the energy equation (Eq. (3.1.3)) yields

$$D(s_1/c_p)/D\theta = -(\kappa_s/\tau_s)t_{\infty,1}/t_{\infty,o} \tag{3.1.6}$$

Thus, the system model depends on a single time constant, τ_s/κ_s. This time constant is the ratio of the heat transfer time constant to the soot particle mass fraction.

These equations are simplified further using small perturbation thermodynamic relations. The ideal gas entropy equation is, for small perturbations using Eq. (2.1.8),

$$\frac{s_1}{c_p} = \frac{p_1}{\gamma p_o} - \frac{\rho_1}{\rho_o} \tag{3.1.7}$$

Also, using Eq. (2.1.5), for small perturbations the gas equation of state is

$$\frac{p_1}{p_o} = \frac{\rho_1}{\rho_o} + \frac{t_{\infty,1}}{t_{\infty,o}} \tag{3.1.8}$$

Equations (3.1.7) and (3.1.8) are substituted into Eq. (3.1.6) to determine the response of the gas temperature to a pressure perturbation. Thus,

$$\frac{D}{D}\left(\frac{s_1}{c_p}\right) = \frac{D}{D\theta}\left(\frac{p_1}{\gamma p_o} - \frac{\rho_1}{\rho_o}\right) = \frac{D}{D\theta}\left[\frac{(1-\gamma)}{\gamma p_o}\, p_1 + \frac{t_{\infty,1}}{t_{\infty,o}}\right] = -\left(\frac{\kappa_s}{\tau_s}\right)\frac{t_{\infty,1}}{t_{\infty,o}} \tag{3.1.9}$$

From Eq. (3.1.9) the desired relation is

$$\left(\frac{D}{D\theta} + \frac{\kappa_s}{\tau_s}\right)\frac{t_{\infty,1}}{t_{\infty,o}} = -\frac{D}{D\theta}\left(\frac{1-\gamma}{\gamma}\right)\frac{p_1}{p_o} \tag{3.1.10}$$

To remove the density perturbation, Eq. (3.1.7) is substituted into Eq. (3.1.1). Thus

$$\frac{D}{D\theta}\left(\frac{p_1}{\gamma p_o} - \frac{s_1}{c_p}\right) + c_o \frac{\partial}{\partial x}\left(\frac{u_1}{c_o}\right) = 0 \qquad (3.1.11)$$

Solving Eq. (3.1.11) for $D(s_1/c_p)/D\theta$ yields

$$\frac{D}{D\theta}\left(\frac{s_1}{c_p}\right) = \frac{D}{D\theta}\left(\frac{p_1}{\gamma p_o}\right) + c_o \frac{\partial}{\partial x}\left(\frac{u_1}{c_o}\right) \qquad (3.1.12)$$

Equations (3.1.2), (3.1.6), (3.1.10), and (3.1.12) are the fundamental model equations. These equations are next written in state variable form using acoustic pressure, particle velocity, entropy, and gas temperature as the state variables. Then a solution to the model differential equation is derived.

2. State Variable Formulation

The system differential equation based on the small perturbation approximation is discussed next. Equations (3.1.2), (3.1.6), (3.1.10), and (3.1.12) are written in state variable form as

$$A \frac{\partial}{\partial \theta} \vec{q} + Bu_o \frac{\partial}{\partial x} \vec{q} + \vec{C}q = 0 \qquad (3.1.13)$$

where

$$A = \begin{bmatrix} 1-\gamma & 0 & 0 & 1 \\ 0 & 1 & 0 & 0 \\ 0 & 0 & 1 & 0 \\ 1 & 0 & -1 & 0 \end{bmatrix} \qquad (3.1.14)$$

$$B = \begin{bmatrix} 1-\gamma & 0 & 0 & 1 \\ c_o/u_o & 1 & 0 & 0 \\ 0 & 0 & 1 & 0 \\ 1 & c_o/u_o & -1 & 0 \end{bmatrix} \tag{3.1.15}$$

$$C = \begin{bmatrix} 0 & 0 & 0 & \kappa_s/\tau_s \\ 0 & 0 & 0 & 0 \\ 0 & 0 & 0 & \kappa_s/\tau_s \\ 0 & 0 & 0 & 0 \end{bmatrix} \tag{3.1.16}$$

$$\vec{q} = \begin{bmatrix} p_1/\gamma p_o \\ u_1/c_o \\ s_1/c_p \\ t_{\infty,1}/t_{\infty,o} \end{bmatrix} \tag{3.1.17}$$

The state variable solution to Eq. (3.1.13) is assumed to have the form

$$q_j(x,\theta) = \sum_{\ell=1}^{4} \eta_{j\ell} e^{(ik_o\Omega)_\ell x - i\omega\theta} \tag{3.1.18}$$

Taking the Fourier transform in the time variable and the space variable of Eq. (3.1.13) produces a set of four homogeneous algebraic equations in four unknowns expressed by the following matrix equation

$$\left[A(-i\omega) + B(ik_o\Omega)u_o + C\right]Q\left[(-i\omega), (ik_o\Omega)\right] \qquad (3.1.19)$$

A non-trivial solution to Eq. (3.1.19) exists if and only if the following determinant of the coefficient matrix vanishes:

$$\begin{bmatrix} \Delta(1-\gamma) & 0 & 0 & \Delta + \frac{\kappa_s}{\tau_s} \\ (i\kappa_o\Omega)c_o & \Delta & 0 & 0 \\ 0 & 0 & \Delta & \kappa_s/\tau_s \\ \Delta & c_o(i\kappa_o\Omega) & -\Delta & 0 \end{bmatrix} = 0 \qquad (3.1.20)$$

where

$$\Delta - (-i\omega) + (i\kappa_o\Omega)u_o \qquad (3.1.21)$$

Solving the determinant equation yields a third-order polynomial wave number equation for $(i\kappa_o\Omega)$,

$$\left(\frac{\Delta}{c_o}\right)^2\left[1 - \frac{(1-\gamma)}{\left(1 + \frac{\tau_s\Delta}{\kappa_s}\right)}\right] = (i\kappa_o\Omega)^2 \qquad (3.1.22)$$

and a solution $\Delta = 0$ which corresponds to a wavenumber

$$(i\kappa_o\Omega)_a^o = \frac{i\omega}{u_o} \qquad (3.1.23)$$

The roots of the third-order polynomial equation can be found numerically to great accuracy using an iteration method due to Muller (Conte

and de Boor (1972)). For the data studied herein the Mach number is low and a good approximate solution at all frequencies is

$$(i\kappa_o\Omega)_b^o = -\frac{\kappa_s}{\tau_s u_o} + \frac{i\omega}{u_o} \tag{3.1.24}$$

$$(i\kappa_o\Omega)^+ = \frac{i(\omega/c_s)}{1 + M_s} \tag{3.1.25}$$

$$(i\kappa_o\Omega)^- = -\frac{i(\omega/c_s)}{1 - M_s} \tag{3.1.26}$$

where

$$c_s = \frac{c_o}{\left[1 + \frac{(\gamma - 1)}{\left(1 + (-i\omega)\frac{\tau_s}{\kappa_s}\right)}\right]} \tag{3.1.27}$$

and

$$M_s = \frac{u_o}{c_s} \tag{3.1.28}$$

The state variable solution to Eq. (3.1.13) is expressed in terms of four one-dimensional normal modes with wave numbers given by Eqs. (3.1.23) to (3.1.26). Equations (3.1.25) and (3.1.26) indicate that two modes may be interpreted as acoustic modes corresponding to right and left traveling acoustic waves. The remaining modes represent waves traveling with the flow. The wave defined by Eq. (3.1.23) is attenuated. However, this is not true for the wave defined by Eq. (3.1.24) since τ_s/κ_s is assumed to be small. Thus, the attenuation of the wave

traveling with the flow calculated by substituting Eq. (e.1.24) into Eq. (2.1.46) is very large and this wave is highly damped for the cases considered herein. Consequently, this mode quickly decays in the combustion duct system. The wave with wave number given by Eq. (3.1.23) is assumed to have negligible effect on the system. Thus, the pressure and particle velocity and the structure of the pressure auto-spectra and cross-spectra are assumed to be determined only by the acoustic modes.

The state variable differential equation (Eq. (3.1.13)) depends upon four dependent variables: pressure, particle velocity, entropy, and bulk gas temperature. In the next section the non-acoustic modes are removed from this state variable differential equation. This produces an acoustic state variable system differential equation which has two independent variables: pressure and particle velocity. However, the new acoustic wave number solutions are identical to the previous ones. The acoustic state variable system differential equation is further simplified by use of a velocity potential function to create a single one-dimensional differential equation. This is the equation used to model the system.

3. Acoustic State Variable Formulation

The set of differential equations which has only the acoustic mode is obtained by neglecting the convection term, $u_o \partial s/\partial x$ in Eq. (3.1.6). As a consequence Eq. (3.1.9) becomes

$$\frac{d}{d\theta}\left(\frac{s_1}{c_p}\right) = \frac{d}{d\theta}\left[\frac{(1-\gamma)}{\gamma}\frac{p_1}{p_o} + \frac{t_{\infty,1}}{t_{\infty,o}}\right] = -\frac{\kappa_s}{\tau_s}\frac{t_{\infty,1}}{t_{\infty,o}} \qquad (3.1.29)$$

From this equation the response of the bulk gas temperature to a pressure perturbation is

$$\left(\frac{d}{d\theta} + \frac{\kappa_s}{\tau_s}\right)\frac{t_{\infty,1}}{t_{\infty,o}} = -\frac{d}{d\theta}\left(\frac{1-\gamma}{\gamma}\right)\frac{p_1}{p_o} \tag{3.1.30}$$

Taking the Fourier transform in the time domain in Eqs. (3.1.29) and (3.1.30) yields

$$\Phi\left[\frac{t_{\infty,1}}{t_{\infty,o}}\right] = -\frac{(-i\omega)(1-\gamma)}{\left[(-i\omega) + \frac{\kappa_s}{\tau_s}\right]}\Phi\left[\frac{p_1}{\gamma p_o}\right] \tag{3.1.31}$$

and

$$\Phi\left[\frac{s}{c_p}\right] = \frac{\mathcal{J}(\omega)}{c_p}\Phi\left[\frac{p_1}{\gamma p_o}\right] \tag{3.1.32}$$

where

$$\frac{\mathcal{J}(\omega)}{c_p} \quad \frac{(1-\gamma)}{1 + (-i\omega)\frac{\kappa_s}{\tau_s}} \tag{3.1.33}$$

The time Fourier transform of Eq. (3.1.1) is

$$\left[(-i\omega) + u_o\frac{\partial}{\partial x}\right]\Phi\left[\frac{u_1}{c_o}\right] + c_o\frac{\partial}{\partial x}\Phi\left[\frac{p_1}{\gamma p_o}\right] = 0 \tag{3.1.34}$$

Substituting Eq. (3.1.32) into the time Fourier transform of Eq. (3.1.12) yields

$$\left[(-i\omega) + u_o\frac{\partial}{\partial x}\right]\left[1 - \frac{\mathcal{J}(\omega)}{c_p}\right]\Phi\left[\frac{p_1}{\gamma p_o}\right] + c_o\frac{\partial}{\partial x}\Phi\left[\frac{u_1}{c_o}\right] = 0 \tag{3.1.35}$$

A plane wave solution to Eqs. (3.1.34) and (3.1.35) can be obtained in terms of a velocity potential, ψ, where

$$u_1 = -\frac{\partial \psi}{\partial x} \tag{3.1.36}$$

and

$$p_1 = \rho_o \left(\frac{\partial}{\partial \theta} + u_o \frac{\partial}{\partial x}\right)\psi \tag{3.1.37}$$

Substituting the time Fourier transform of Eqs. (3.1.36) and (3.1.37) into Eq. (3.1.35) yields a new governing partial differential equation called the non-adiabatic velocity potential wave equation

$$L\Phi[\psi] = \left[(-ik_s) + M_s \frac{d}{dx}\right]^2 \Phi[\psi] - \frac{d^2}{dx^2}\Phi[\psi] = 0 \tag{3.1.38}$$

where

$$c_s = \frac{c_o}{\left[1 - \frac{\mathcal{J}(\omega)}{c_p}\right]^{1/2}} \tag{3.1.39}$$

and

$$k_s = \frac{\omega}{c_s} \tag{3.1.40}$$

The velocity potential solution is assumed to be proportional to $\exp((ik_o\Omega)x - i\omega\theta))$. Substituting this solution into Eq. (3.1.38) yields a wave number equation which has the acoustic wave numbers given by Eqs. (3.1.25) and (3.1.26) as a solution. Consequently, the velocity

potential wave equation solution consists of an acoustic wave traveling upstream and downstream expressed as

$$\psi = \left[ae^{(ik_o\Omega)^+ x} + be^{(ik_o\Omega)^- x} \right] e^{-i\omega\theta} \qquad (3.1.41)$$

In the following sections the use of the Fourier transform operator notation is discontinued and all variables such as ψ, p, and u are Fourier transformed variables. The following sections apply the acoustic state vector formulation and the velocity potential definition to the study of sound propagation in the ducted combustion system.

B. Application to Ducted Combustion System

The analysis developed in the last section is now used to study the spectral structure of pressure measurements made in the ducted combustion system shown in Figure 5. The ducted combustion system shown in Figure 5 consists of: (1) a source region inside the combustor can, (2) a non-source region inside a spool piece and a long duct, (3) an area expansion and contraction on either side of the spool piece, and (4) a downstream boundary at the exit of the long duct and an upstream boundary at the combustor inlet.

The solution for the velocity potential in a non-source region is given by Eq. (3.1.41). The velocity potential wave equation (Eq. (3.1.38)) is assumed to apply in the source region with the addition of a source term $G(\omega,x)$ on the right-hand side. Using the combustor inlet and exit impedance as a boundary condition, a unique Green's function solution for the velocity potential is found. The acoustic pressure and particle velocity can be found from a velocity potential solution using Eqs. (3.1.36) and (3.1.37). Consequently, the acoustic

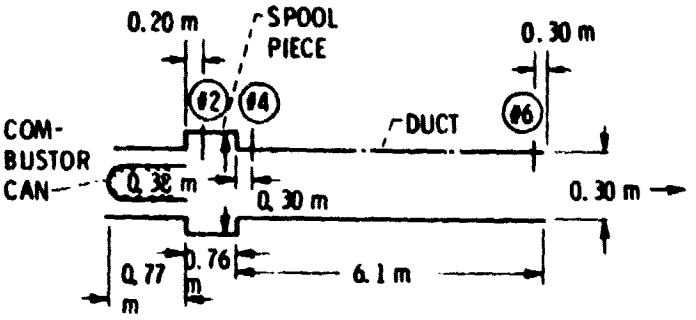

Figure 5. - Ducted combustion system.

pressure and particle velocity at the combustor exit can be determined from the velocity potential solution in the combustor. The acoustic pressure and particle velocity at the combustor exit can then be used to find the acoustic pressure and particle velocity at any other point in the ducted combustor system with four-pole equations in transmission matrix form derived using Eqs. (3.1.36), (3.1.37), and (3.1.41). The combustor exit impedance can be calculated from the duct exit impedance using the same four-pole transmission matrix equations. The transmission matrix approach is discussed by Parrott (1973, Lampton (1978), Igarashi and Toyama (1958), Miwa and Igarashi (1959), and Igarashi and Arai (1960).

Details of the mathematical models used in calculating the auto-spectra and cross-spectra are presented in the following sections. The next section discusses the source region.

1. Source Region

The acoustic state vector approach developed in the last section is used to study the spectral structure of pressure measurements made in the ducted combustion system. The linear non-homogeneous velocity potential wave equation assumed to apply in the source region is

$$L\psi = G(\omega,x) \tag{3.2.1}$$

The boundary conditions at the combustor inlet and exit are, respectively,

$$\frac{Z_{C1}}{\rho_o c_o} = \frac{1}{\rho_o c_o}\frac{p_1}{u_1}\bigg|_{x=0} \tag{3.2.2}$$

and

$$\frac{Z_{CE}}{\rho_o c_o} = \frac{1}{\rho_o c_o} \frac{p_1}{u_1}\bigg|_{x=L_c} \tag{3.2.3}$$

In the following analysis, the combustion noise source is assumed to be acoustically compact in the x-direction. That is, the size of the source region is assumed small in comparison with the length of the waves generated. The volume source-distribution of monopole order confined to the duct cross-section $x = x_\ell$ is written as

$$G(\omega,x) = C_o \mathscr{H}(\omega)\delta(x - x_\ell)\left(1 - M_s^2\right) \tag{3.2.4}$$

Similar source descriptions have been previously applied by Mani (1978) to a fan noise problem and by Morfey (1971), Ingard and Singhal (1975, and Swinbanks (1975) to duct noise source problems.

Substituting Eqs. (3.1.38) and (3.2.4) into Eq. (3.2.1), and the time Fourier transforms of Eqs. (3.1.36) and (3.1.37) into Eqs. (3.2.2) and (3.2.3) and some algebraic manipulation yields a mathematical problem that has the form of a general second-order Sturm-Liouville differential equation with unmixed boundary conditions:

$$\mathscr{L}\psi = -\frac{d}{dx}\left(\varepsilon \frac{d\psi}{dx}\right) + \zeta\psi = \varepsilon C_o \mathscr{H}(\omega)\delta(x - x_\ell) \tag{3.2.5}$$

$$\mathscr{B}_{CI}(0) = \left\{\left[\frac{Z_{CI}}{\rho_o c_o} + M_o\right]\frac{d\psi}{dx} + (-ik_o)\psi\right\}\bigg|_{x=0} = 0 \tag{3.2.6}$$

$$\mathscr{B}_{CE}(L_c) = \left\{\left[\frac{Z_{CI}}{\rho_o c_o} + M_o\right]\frac{d\psi}{dx} + (-ik_o)\psi\right\}\bigg|_{x=L_c} = 0 \tag{3.2.7}$$

where

$$c = e^{-\left[\frac{2(-ik_s M_s)}{1 - M_s^2}\right]x} \tag{3.2.8}$$

and

$$\zeta = \frac{\varepsilon(-ik_s)^2}{1 - M_s^2} \tag{3.2.9}$$

However, since the differential equation has complex coefficients the operator $\mathscr{L}$ is not self-adjoint or Hermitian.

Since the differential equation is not self-adjoint, the development of a solution in terms of an orthogonal set of eigenfunctions is more complex than obtaining a solution by constructing the Green's function solution (see Swinbanks (1975), Morse and Feshback (1953), pp. 884-886), and Kraft (1977)). The Green's function solution is constructed using the two initial value solutions of the homogeneous equation

$$\mathscr{L}\psi = 0 \tag{3.2.10}$$

which satisfy Eqs. (3.2.6) and (3.2.7). This method is described by Morse and Feshback (1956, pp. 523-530) and Friedman (1956) who apply it to self-adjoint operators. The solution to Eq. (3.2.10) with boundary condition given by Eq. (3.2.6) is

$$\psi_{CI} = a\left[e^{(ik_o\Omega)^+ x} + R_{CI}e^{(ik_o\Omega)^- x}\right] \tag{3.2.11}$$

where

$$R_{CI} = \frac{\left[\left(\frac{Z_{CI}}{\rho_o c_o} + M_o\right)\Omega^+ - 1\right]}{\left[1 - \Omega^-\left(M + \frac{Z_{CI}}{\rho_o c_o}\right)\right]} \tag{3.2.12}$$

The solution to Eq. (3.2.10) with boundary condition given by Eq. (3.2.7) is

$$\psi_{CE} = a_{CE}\left[e^{(ik_o\Omega)^+x} + R_{CE}e^{(ik_o\Omega)^-x}\right] \tag{3.2.13}$$

where

$$R_{CE} = \frac{\left[\left(\frac{Z_{CE}}{\rho_o c_o} + M_o\right)\Omega^+ - 1\right]}{\left[1 - \Omega^-\left(M_o + \frac{Z_{CE}}{\rho_o c_o}\right)\right]} e^{ik_o(\Omega^+ - \Omega^-)L_o} \tag{3.2.14}$$

Consequently, the Green's function solution to Eqs. (3.2.5) to (3.2.7) is given by

$$\mathcal{G}(\omega, x, x_\ell) = \begin{cases} -C_o\mathcal{H}(\omega)\dfrac{\psi_{CE}(x_\ell)\psi_{CI}(x)}{W(x_\ell)} & 0 < x < x_\ell < L_c \\ -C_o\mathcal{H}(\omega)\dfrac{\psi_{CI}(x_\ell)\psi_{CE}(x)}{W(x_\ell)} & 0 < x_\ell < x < L_c \end{cases} \tag{3.2.15}$$

where $W(x)$ is the Wronskian

$$W(x) = \psi_{CI}\frac{d\psi_{CE}}{dx} - \psi_{CE}\frac{d\psi_{CI}}{dx} \tag{3.2.16}$$

Using the time Fourier transforms of Eqs. (3.1.36) and (3.1.37), the pressure and particle velocity Fourier transforms at the combustor exit are

$$p_1 = \rho_o\left[(-i\omega) + u_o \frac{\partial}{\partial x}\right]\mathcal{G}(\omega,x,x_\ell)\Big|_{x=L_c} \tag{3.2.17}$$

and

$$u_1 = -\frac{\partial}{\partial x}\mathcal{G}(\omega,x,x_\ell) \tag{3.2.18}$$

Equations (3.2.17) and (3.2.18) define the acoustic state vector at the combustor exit determined from the combustor inlet and exit boundary conditions and the source spectrum. Relating the acoustic state vector at the combustor exit to the acoustic state vector at any other point outside the source region is done using an acoustic transmission matrix. The acoustic transmission matrix is based on the solution to the homogeneous wave equation and it will be discussed next.

2. Duct Acoustic Transmission Matrix

The duct acoustic transmission matrix relates the acoustic pressure and particle velocity at one point in the duct to the acoustic pressure and particle velocity at another point providing neither point is in a source region and the duct has a constant area. It is calculated as follows.

Substituting Eq. (3.1.41) into Eqs. (3.1.36) and (3.1.37) yields the pressure and particle velocity equations

$$p_1 = \rho_o c_o(-ik_o)\left[a_{11}^{ae}e^{(ik_o\Omega)^+x} + a_{12}^{be}e^{(ik_o\Omega)^-x}\right] \tag{3.2.19}$$

and

$$u_1 = (ik_o)\left[a_{21}ae^{(ik_o\Omega)^+x} + a_{22}be^{(ik_o\Omega)^-x}\right] \tag{3.2.20}$$

where

$$a_{11} = 1 - M_o\Omega^+ \tag{3.2.21}$$

$$a_{12} = 1 - M_o\Omega^- \tag{3.2.22}$$

$$a_{21} = \Omega^+ \tag{3.2.23}$$

and

$$a_{22} = \Omega^- \tag{3.2.24}$$

The integration constants a and b in Eqs. (3.2.19) and (3.2.20) are determined by assuming that x = 0, p = p(0), and u = u(0) at the upstream boundary and x = L, p = p(L), and u = u(L) at the downstream boundary. As a consequence, the relation between the acoustic state vector at x = 0, y(0) and the acoustic state vector at L, Y(L) is

$$\vec{Y}(L) = \begin{pmatrix} p_1 \\ u_1 \end{pmatrix}_{x=L} = \begin{bmatrix} \alpha_{11} & \alpha_{12} \\ \alpha_{21} & \alpha_{22} \end{bmatrix} \begin{pmatrix} p_1 \\ u_1 \end{pmatrix}_{x=0} = \left[\alpha_{m,n}\right]\vec{Y}(0) \tag{3.2.25}$$

where

$$\alpha_{11} = \frac{a_{11}a_{22}e^{(ik_o\Omega)^+L_c} - a_{12}a_{21}e^{(ik_o\Omega)^-L_c}}{a_{11}a_{22} - a_{21}a_{12}} \tag{3.2.26}$$

$$a_{12} = \rho_o c_o \frac{\left[-a_{11}a_{12}e^{(ik_o\Omega)^+L_c} + a_{11}a_{12}e^{(ik_o\Omega)^-L_c}\right]}{a_{11}a_{22} - a_{21}a_{12}} \qquad (3.2.27)$$

$$a_{21} = \frac{\left[a_{21}a_{22}e^{(ik_o\Omega)^+L_c} - a_{22}a_{21}e^{(ik_o\Omega)^-L_c}\right]}{\rho_o c_o (a_{11}a_{22} - a_{21}a_{12}} \qquad (3.2.28)$$

and

$$a_{22} = \frac{-a_{21}a_{12}e^{(ik_o\Omega)^+L_c} + a_{11}a_{22}e^{(ik_o\Omega)^-L_c}}{a_{11}a_{22} - a_{21}a_{12}} \qquad (3.2.29)$$

Now that the transmission matrix between two points in a constant area duct has been derived, it is necessary to discuss the transmission matrix that applies across a discontinuity.

3. Discontinuity Transmission Matrix

The four-pole transmission matrix used at the junction of two pipes of different diameter is based on an acoustic energy conservation law. Various definitions for the acoustic energy in flowing fluids are given by Morfey (1971), Möhring (1971), Candel (1975), Eversman (1979), Tester (1973), and Bergman (1946). While none of these definitions is applicable to a plane wave propagating through a soot particle cloud in a flowing field, the method for finding an energy conservation equation used by Morfey (1971) and by Bergman (1946) is applicable. The relationship which has the form of an acoustic energy conservation law is derived using Eqs. (3.1.34) and (3.1.35). A quantity corresponding to acoustic energy flux is defined by

$$N = \mathcal{J}_1 w_1 \tag{3.2.30}$$

where the acoustic energy per unit mass is

$$\mathcal{J}_1 = u_o u_1 + p_1/\rho_o \tag{3.2.31}$$

and the mass flux fluctuation rate is

$$w_1 = \rho_o u_1 + u_o \rho_1 \tag{3.2.32}$$

If Eq. (3.1.34) is multiplied by ω/c_o and Eq. (3.1.35) by $\mathcal{J}_1/c_o^2$, the sum of the resulting second-order equations can be put in the form

$$(-i\omega)\frac{E}{c_o^2} + \frac{d}{dx}\left(\frac{N}{\rho_o c_o}\right) = 0 \tag{3.2.33}$$

where E represents an acoustic energy density

$$\frac{E}{c_o^2} = \left(\frac{u_1}{c_o}\right)^2 + 2\left[1 - \frac{\mathcal{J}(\omega)}{c_p}\right]\left(\frac{u_o}{c_o}\right)\left(\frac{p_1}{\gamma p_o}\right)\left(\frac{u_1}{c_o}\right) + \left[1 - \frac{\mathcal{J}(\omega)}{c_p}\right]\left(\frac{p_1}{\gamma p_o}\right)^2 \tag{3.2.34}$$

$$\frac{N}{\rho_o c_o} = c_o\left(\frac{\mathcal{J}_1}{c_o^2}\right)\left(\frac{w_1}{c_o}\right) \tag{3.2.35}$$

Integrating Eq. (3.2.33) over a volume yields

$$\int_V (-i\omega)\frac{E(\omega)}{c_o^2}\,dV + \int_S \vec{N}\cdot\hat{n}\,d\sigma = 0 \tag{3.2.36}$$

since

$$\int \nabla\cdot\vec{F}\,dV = \int_S \vec{F}\cdot\hat{n}\,d\sigma \tag{3.2.27}$$

The area discontinuity can be assumed to take place sharply at the junction of two pipes with different diameters causing the flowing gas to undergo a sudden expansion or contraction. As a consequence of Eq. (3.2.36), across the pipe discontinuity the acoustic energy is constant

$$N(1)S(1) = N(2)S(2) \tag{3.2.38}$$

To derive a transmission matrix across the discontinuity Eq. (3.2.38) is rewritten as

$$\mathcal{J}_1(1) = \mathcal{J}_1(2) \tag{3.2.39}$$

and

$$S(1)w_1(1) = S(2)w_1(2) \tag{3.2.40}$$

Algebraic manipulation shows that the acoustic state vectors on either side of the discontinuity are related by

$$\vec{Y}(x_1) = [B_{m,n}]\vec{Y}(x_2) \tag{3.2.41}$$

where the resulting transmission matrix is given by

$$[B_{m,n}] = \begin{bmatrix} 1 & \dfrac{\rho_o c_s M_s(2)\left[1 - \left[\dfrac{S(2)}{S(1)}\right]^2\right]}{1 - \left[\dfrac{S(2)}{S(1)} M_s(2)\right]^2} \\ 0 & \dfrac{S(2)\left[1 - M_s^2(2)\right]}{S(1)\left\{1 - \left[\dfrac{S(2)}{S(1)} M_s(2)\right]^2\right\}} \end{bmatrix} \tag{3.2.42}$$

The next section discusses the last step in formulating the model which is the specification of boundary conditions at the combustor inlet and the duct exit.

4. System Boundary Conditions

First, the boundary condition at the duct exit is discussed. Experimental investigations of the exit impedance of flow ducts reported by Mechel, Schilz, and Dietz (1965) and Cummings (1978) show the duct exit pressure reflection factor may be greater than unity. Theoretical investigations reported by Lumsdaine (1977), Lumsdaine and Ragab (1977), and Mungur and Plumblee (1979) show that the pressure reflection factor is greater than unity because of the flow field at the duct exit. The following empirical expression for $|R|$ is given by Ingard and Singhal (1975)

$$|R| = 0.95 \left[\frac{(1 - M_o)}{(1 + M_o)}\right]^{1.33} \qquad kr_d < 0.5 \tag{3.2.43}$$

where $|R|$ is measured at the upstream end of a duct. In the case of jet exit flow, M_o is replaced by $-M_o$ (Lumsdaine (1977)). For the case studied herein $|R|$ is about 1.03.

The model calculations shown are made using the following combustion duct exit pressure reflection factor

$$R = |R|e^{i\phi} = -\frac{(1 - M_o)}{(1 - M_o)}\left(\frac{1 - \frac{Z}{\rho_o c_o}}{1 + \frac{Z}{\rho_o c_o}}\right) \tag{3.2.44}$$

the duct exit impedance is

$$\frac{Z}{\rho_o c_o} = M + \left[1 - 2\frac{J_1(\nu)}{\nu}\right] - i2\frac{S_1(\nu)}{\nu} \qquad (3.2.45)$$

where

$$\nu = 2kr_d \Big/ \sqrt{1 - M_o^2} \qquad (3.2.46)$$

$J_1(\nu)$ is the Bessel function of the first order and first kind, $S_1(\nu)$ is the Struve function of the first kind and first order, and r_d is the duct radius. The duct exit impedance used was derived by Lumsdaine and Ragab (1977) for a circular duct with flow having an open end fitted with an infinite acoustically rigid flange. Again, in the case of jet exit flow, M_o is replaced by $-M_o$ in Eqs. (3.2.44) to (3.2.46).

The other boundary condition is specified at the combustor entrance. To model the impedance the combustor entrance is taken to be closed by a rigid circular plate at the entrance. This corresponds to a zero particle velocity at $x = 0$. Consequently, the pressure reflection factor is unity at $x = 0$.

Now that the elements that are needed to calculate pressure autospectra and cross-spectra have been described, the calculation procedure will be presented.

C. Calculation Procedure

The following procedure is used to calculate the pressure spectrum. It is applied at each frequency as necessary to obtain the desired spectrum. First, the exit pressure perturbation is arbitrarily assumed to be one Pascal. Then using the duct exit acoustic impedance based on the duct exit pressure reflection factor given by Eqs. (3.2.44) to (3.2.46), the particle velocity is calculated. Next, using the duct

transmission matrix and the area discontinuity transmission matrix as necessary the acoustic state vector at the duct exit is used to find the acoustic state vector at the combustor exit. The resulting acoustic pressure and particle velocity are used to calculate the combustor exit impedance.

The next phase uses this impedance, the combustor entrance impedance, and a white noise source spectrum to determine the velocity potential solution in the source region. This velocity potential solution is used to calculate the acoustic pressure and particle velocity at the combustor exit due to the specified source and boundary conditions.

The last phase uses the duct transmission matrix and the area discontinuity transmission matrix as necessary to calculate the acoustic state vector at any point in the duct from the acoustic state vector at the combustor exit. The pressure auto-spectra at a given point is calculated from

$$H_{ii}(\omega) = \langle p_1^*(\omega,x_i)p_i(\omega,x_i)\rangle \qquad (3.3.1)$$

and the cross-spectrum between two points is calculated from

$$H_{ij}(\omega) = \langle p_1^*(\omega,x_i)p_1(\omega,x_j)\rangle \qquad (3.3.2)$$

The pressure level at a given frequency is calculated from

$$PL_i(\omega) = 10 \log_{10}[H_{ii}(\omega)] \qquad (3.3.3)$$

In this chapter the acoustic model which will be used to calculate pressure auto and cross spectra has been described. The next chapter will describe the experimental investigation.

Symbols Used in This Chapter

A,B,C,D	matrices
a,b	velocity potential wave equation coefficients
a	pressure and velocity wave equation coefficients
$\mathscr{B}$	boundary condition operator
C_o	source spectrum coefficient
c	sound propagation velocity, m/sec
c_o	isentropic speed of sound, m/sec
c_p	gas specific heat at constant pressure, J/kg-K
d	diameter, m
E	acoustic energy density, J/m^3
f	frequency, Hz
$\mathscr{G}(\omega,x,y)$	solution in source region
$G(\omega,x)$	source term
$\mathscr{H}(\omega)$	source term coefficient
H	heat transfer coeffficient, W/m^2-K
i	$(-1)^{1/2}$
$\mathscr{I}$	energy per unit mass, J/kg
k	propagation wave number, ω/c_o, m^{-1}
L, $\mathscr{L}$	second order space differential equation operator
L_c	combustor length
M	Mach number, u_o/c
m	soot particle mass, kg
Nu_H	heat transfer Nusselt number, Hd/κ
N	acoustic energy flux
n	number of particles per unit volume
PL	pressure level, dB

p	pressure, N/m^2
$\dot{Q}$	heat transferred to gas from particles by convection
$Q(-i\omega, ik_o\Omega)$	time and space Fourier transform of q
$\vec{q}$	system state vector
$\mathcal{R}$	gas constant, J/kg-K
R	reflection factor
r	radius, m
$\mathcal{S}(\omega)/c_p$	entropy source transfer function
S	area, m^2
s	entropy of gas, J/kg-K
t	temperature, K
u	velocity of bulk gas, m/sec
W	Wronskian
w	mass flux, kg/m^2, sec
x	Cartesian coordinate, m
$\vec{Y}$	acoustic state vector
Z	acoustic impedance, mks Rayles
$\alpha_{m,n}$	duct transmission matrix element
$\beta_{m,n}$	discontinuity transmission matrix element
γ	specific heat ratio of gas
Δ	time and space Fourier transform of D/Dθ
ε	see Eq. (3.2.8)
ζ	see Eq. (3.2.9)
η	see Eq. (3.1.18)
θ	time, sec
κ	gas thermal conductivity, W/m-K
κ_s	soot particle mass fraction, nm/ρ_o

ν	$2\,kr/(1 - M^2)^{1/2}$
ρ	gas density, kg/m
τ_s	soot particle thermal relaxation time, $m_s c_p/4\pi r^2 (Nu_H/d_s)\kappa$
$\Phi[\ \ ]$	Fourier transform operator
ϕ	reflection factor phase angle, deg
ψ	velocity potential function
Ω	velocity potential wave number factor
ω	angular frequency, radians/sec

Superscripts and subscripts:

$\langle\ \rangle$	time average
$(\vec{\ })$	vector quantity
$(\bar{\ })$	instantaneous quantity
$(\ )^-$	upstream propagating
$(\ )^+$	downstream propagating
$(\ )^o$	wave propagating with flow
$(\ )_{CE}$	combustor exit
$(\ )_{CI}$	combustor inlet
$(\ )_d$	exit of duct system
$(\ )_{ij}, (\ )_j$	identifies an axial duct location
$(\ )_\ell$	identifies source location
$(\ )_{m,n}$	elements of a matrix
$(\ )_s$	property of or due to soot particle
$(\ )_o$	reference state quantity
$(\ )_1$	perturbed quantity
$(\ )_\infty$	property far from soot particle

IV. EXPERIMENTAL INVESTIGATION

A. Apparatus, Test Conditions, and Instrumentation

The test facility is shown schematically in Figure 5. The combustor consists of a J-47 burner can placed concentrically in a 0.30 m diameter by 0.77 m long flow duct. The combustor section is followed by a 0.38 m diameter by 0.76 m long spool piece. This section is followed by a 0.30 m diameter by 6.1 m long flow duct. A photograph of the test facility and test site is shown in Figure 6. The nozzle shown mounted to the long duct in Figure 6 was removed for the tests.

The measurements discussed were made at an exit temperature of approximately 920 K and at air mass flow rates of 0.5, 1.13, and 1.68 kg/sec. The corresponding air velocities at the exit of the long duct were 18.5, 41.6, and 61.3 m/sec and the corresponding fuel flow rates were 0.009, 0.018, and 0.027 kg/sec. The fuel-air ratio was about 0.02 for each test condition. Also, at each of these test conditions, the fuel used was a jet aircraft fuel called Jet A.

Simultaneous internal fluctuating pressure measurements were made at the three locations shown in Figure 5. One measurement was made in the spool piece. Two measurements were made in the long duct, one just downstream of the spool piece and one near the nozzle exit plane.

The transducers used were conventional 5/8 cm diameter (nominal) condenser microphones with pressure response cartridges. To preclude exposing the microphones to the high temperature combustion gases in the duct system, the microphones were mounted outside the duct. The

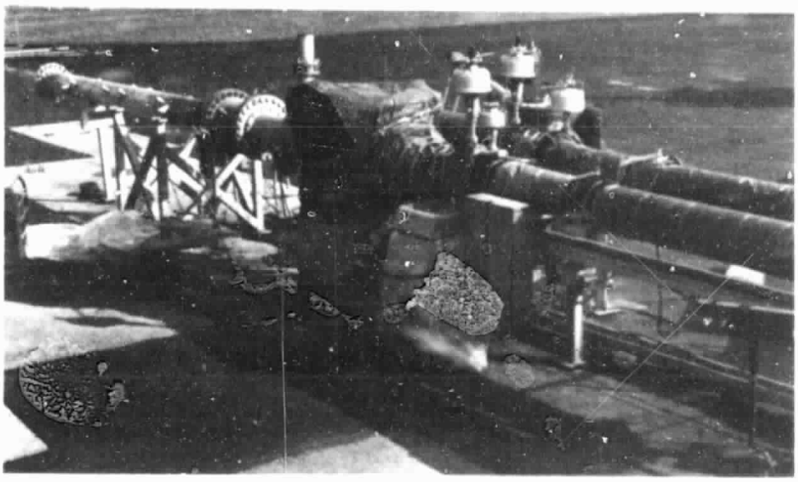

Figure 6. Experimental facility. CS-80-2093

fluctuating static pressure at a given location in the duct system was connected to a microphone by means of a "semi-infinite" acoustic waveguide tube which was a very long piece of narrow tubing. This design eliminated longitudinal resonance and produces an anechoic connection between the duct system and the transducers.

A drawing of a typical probe is shown in Figure 7. The microphone was flush mounted in the acoustic waveguide through a supporting block and housed in a pressure chamber. Attached to the block were a 5/8 cm diameter sensing tube on one end and a coil of tubing of the same diameter, 30 meters long, on the other. The diameter of the coil was approximately 30 cm.

The sensing tube of each probe was flush mounted as a static pressure tap at each measuring location. A regulated nitrogen purge flow was maintained in each sensing line to protect the microphone from hot combustion gases. Since the signals from pairs of probes were to be used to calculate cross-spectra, the regulated purge flow system was separate for each probe. This prevented any common valve noise from the regulator contributing to the cross-spectra. Static pressure was balanced across the microphone by means of a small vent hole connecting the pressure chamber and sensing tube. A schematic of a typical duct probe installation is shown in Figure 8. A photograph of duct probes installed in the spool piece is shown in Figure 9.

The internal probes have previously been used for engine measurements (Karchmer and Reshotko (1976), Reshotko, Karchmer, Penko, and McArdle (1977), and Karchmer, Reshotko, and Montegani (1977) and measurements in a combustion component test facility (Reshotko and Karchmer (1977). Probe design, frequency response, and operating characteristics are discussed by Karchmer (1978).

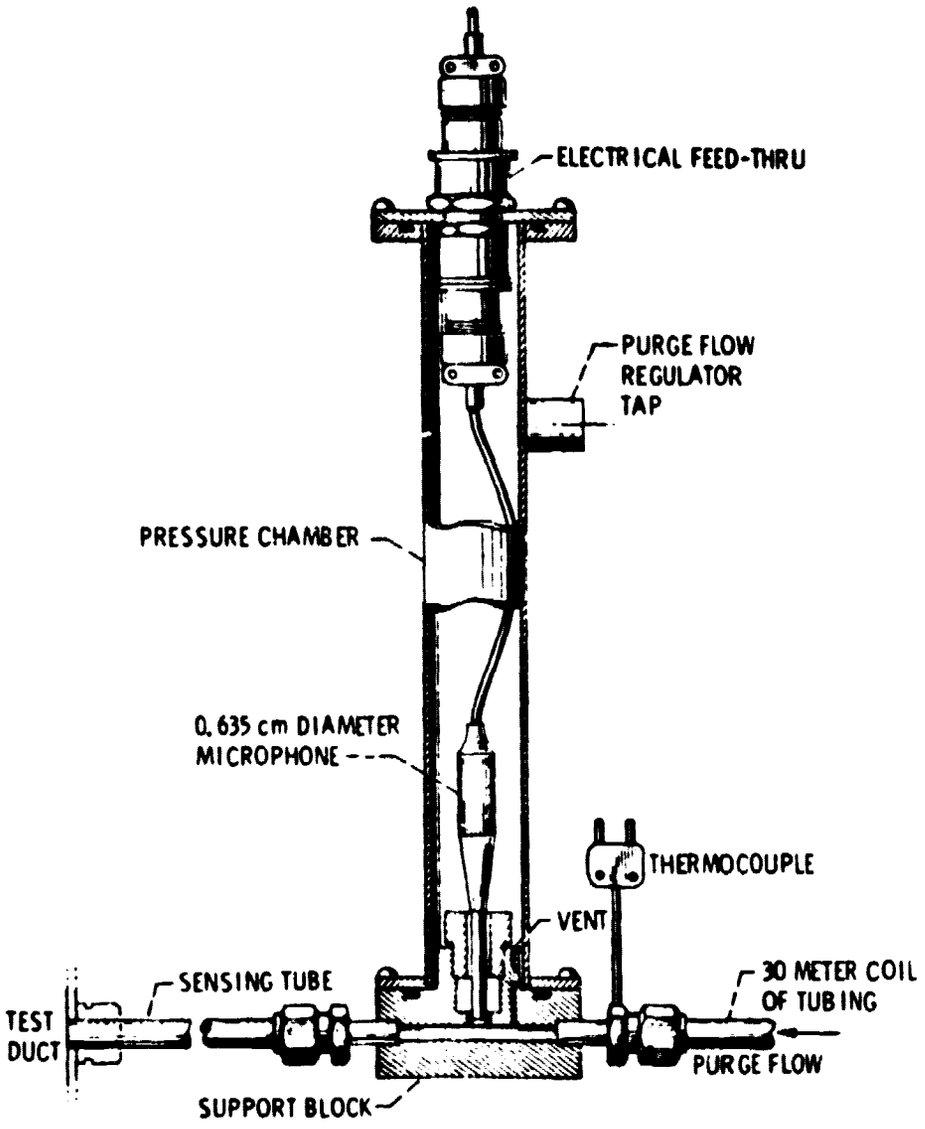

Figure 7. - Duct pressure probe.

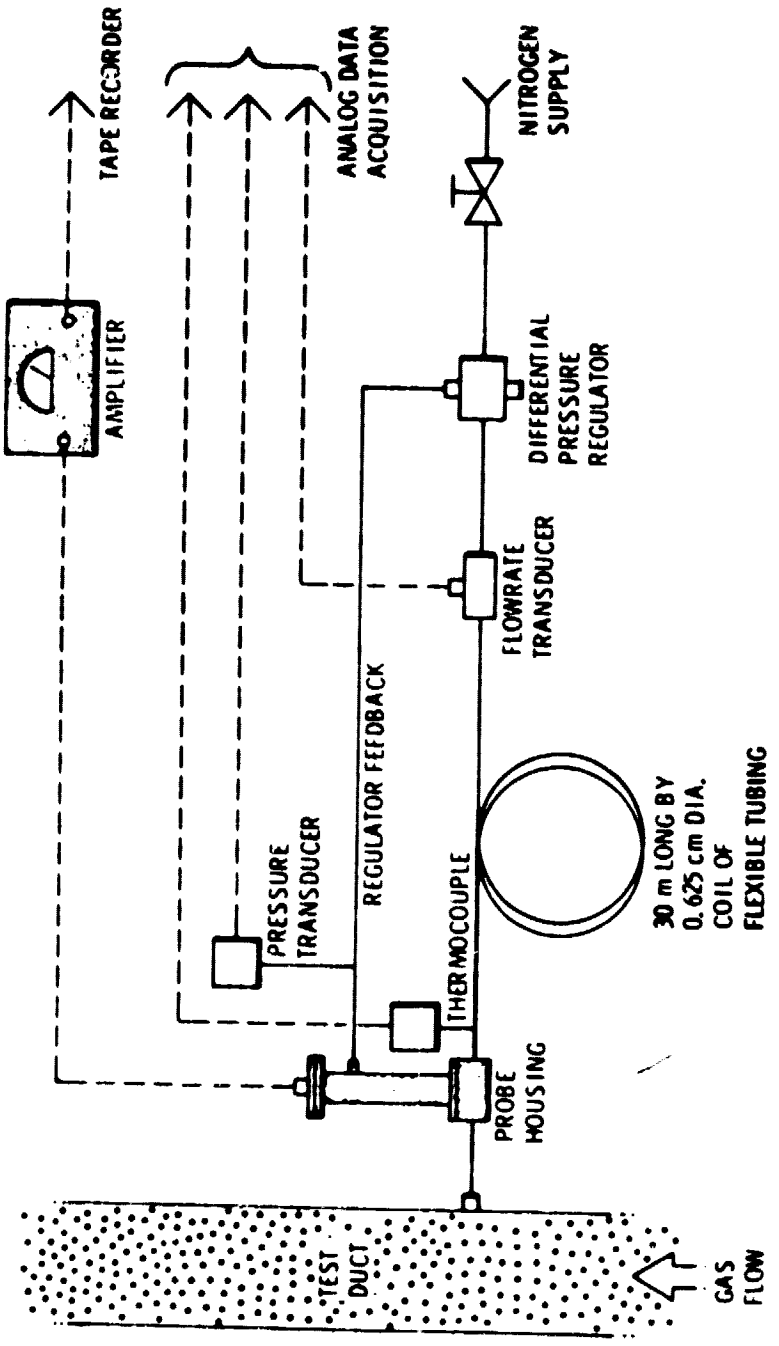

Figure 8. - Schematic of duct probe installation.

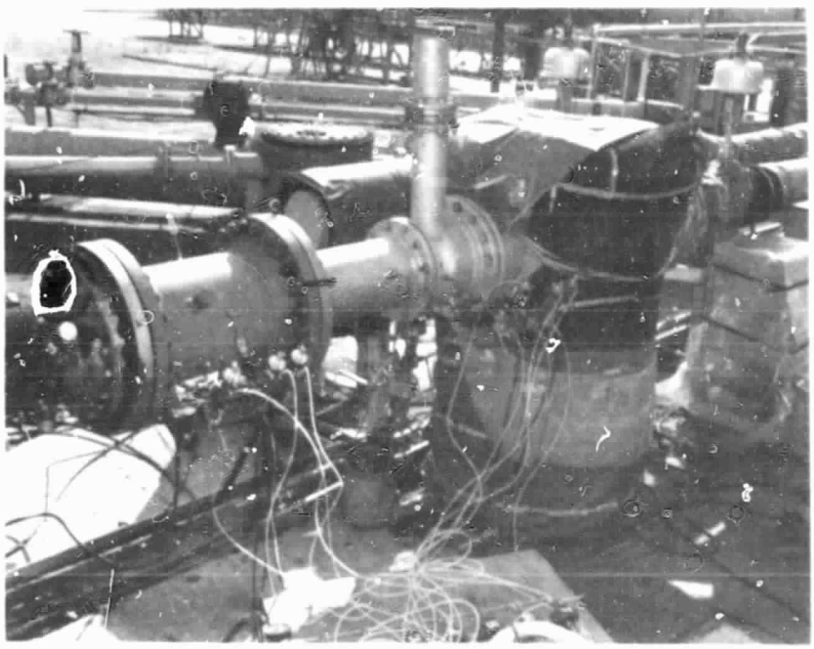

B. Data Acquisition and Processing

As part of the facility start up procedure, the microphones were calibrated with a pistonphone which provided a standard sound pressure level of 124 dB (referenced to 20 μPa) at 250 Hz. Microphone signals were sent over shielded cable to a remote control room for amplification, signal conditioning, and recording on FM magnetic tape. The tape recorder used was equipped with IRIG standard, intermediate band, group II electronics, which provides a flat frequency response to 20 kHz on both record and reproduce at a tape speed of 60 in./sec. The dynamic range available was approximately 48 dB. All signals were recorded on 120 second record lengths for later processing. Record lengths of 120 seconds were used to obtain high statistical confidence in the spectral data. Spectrum function confidence limits are described in Appendix B. All measurement errors are determined by the microphone response which is generally accurate to better than plus or minus 1 dB.

Operating conditions were monitored and recorded on the NASA Lewis CADDE system (Central Automatic Digital Data Encoder). On line data processing and analysis was limited to 1/3 octave-band spectral analysis of the various pressure signals.

All auto-spectra and cross-spectra produced from pressure signals were obtained by off-line processing of the taped signals on a two-channel, FFT (Fast Fourier Transform) digital signal processor, with built-in analog to digital converter and 120 dB/octave anti-aliasing filters. The 99 percent confidence interval for the spectra computed from the taped signals is shown in Appendix B to be better than plus or minus 1.5 dB.

The auto-spectra and cross-spectra considered herein are defined as follows. The finite Fourier transform of time signals $x(\theta)$ and $y(\theta)$ of the record length θ is

$$X_\theta(f) = \int_0^\theta x(\theta)e^{-i2\pi f\theta}\, d\theta \qquad (4.2.1)$$

$$Y_\theta(f) = \int_0^\theta y(\theta)e^{-i2\pi f\theta}\, d\theta \qquad (4.2.2)$$

The two one-sided auto-spectral density functions (also called power-spectral density functions) and the single one-sided cross-spectral density function obtainable from measurement of signals $x(\theta)$ and $y(\theta)$ are defined by the following expressions

$$G_x(f) = \lim_{\theta \to \infty} \frac{2E}{\theta} [X_\theta^*(f)X_\theta(f)] \qquad (4.2.3)$$

$$G_y(f) = \lim_{\theta \to \infty} \frac{2E}{\theta} [Y_\theta^*(f)Y_\theta(f)] \qquad (4.2.4)$$

$$G_{xy}(f) = \lim_{\theta \to \infty} \frac{2E}{\theta} [X_\theta^*(f)Y_\theta(f)]$$

$$= C_{xy}(f) + iQ_{xy} \qquad (4.2.5)$$

where $E[\ ]$ denotes an expected value operation (Bendat and Piersol (1971)). The auto-spectra are shown in the following figures in terms of pressure levels referenced to 20 μPa defined as

$$PL_x = 10 \log_{10}[G_x(f)] \qquad (4.2.6)$$

$$PL_y = 10 \log_{10}[G_y(f)] \qquad (4.2.7)$$

The cross-spectra are shown in the following figures in terms of pressure levels referenced to 20 μPa and phase angles defined as

$$PL_{xy}(f) = 10 \log_{10}\left\{C^2_{xy}(f) + Q^2_{xy}(f)\right\} \qquad (4.2.8)$$

$$\phi_{xy}(f) = \tan^{-1}\left[\frac{Q_{xy}(f)}{C_{xy}(f)}\right] \qquad (4.2.9)$$

C. Measured Pressure Auto-Spectra and Cross-Spectra

Constant bandwidth pressure auto-spectra and cross-spectra measured in the spool piece, near the entrance of the long duct, and near the exit of the long duct are shown in Figures 10 to 13. The spectra at each location have a different structure. However, at each location, the structure of the measured spectra is similar for each test condition. For example, the location of resonance peaks and dips in Figures 10 to 12 is nearly the same for each operating condition. At each location and for all test conditions the peaks and dips tend to be sharper at the low frequencies and broader at the high frequencies.

Constant bandwidth pressure cross-spectra measured across the area contraction at three test conditions are shown in Figures 13(a), (b), and (c), respectively. Both magnitude and phase are shown. The location of the resonance peaks and dips in the magnitude plot of the cross-spectra is nearly the same at each test condition. Also, the peaks and dips again tend to be sharpter at the low frequencies and braoder at the higher frequencies.

The phase plot can be characterized as neither just a negative sloped straight line due to a time delay nor just a curve that varies abruptly between 0 and 180 degrees in a regular manner that would be

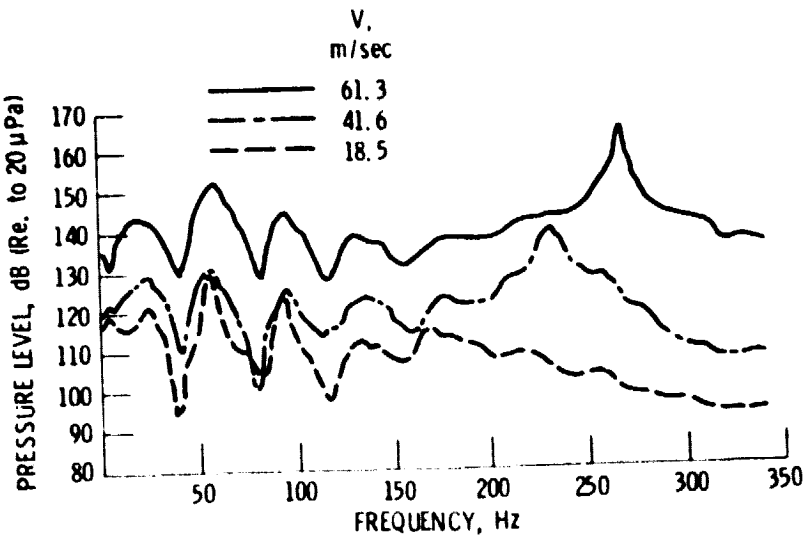

Figure 10. - Pressure auto-spectra measured in spool piece.

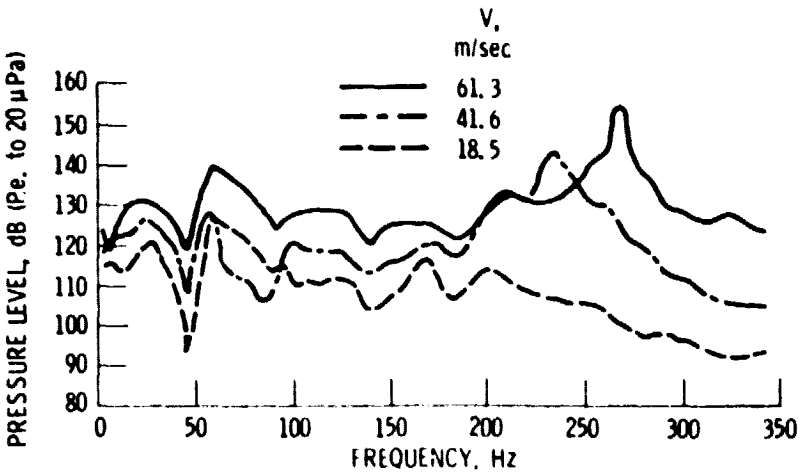

Figure 11. - Pressure auto-spectra measured near entrance of long duct.

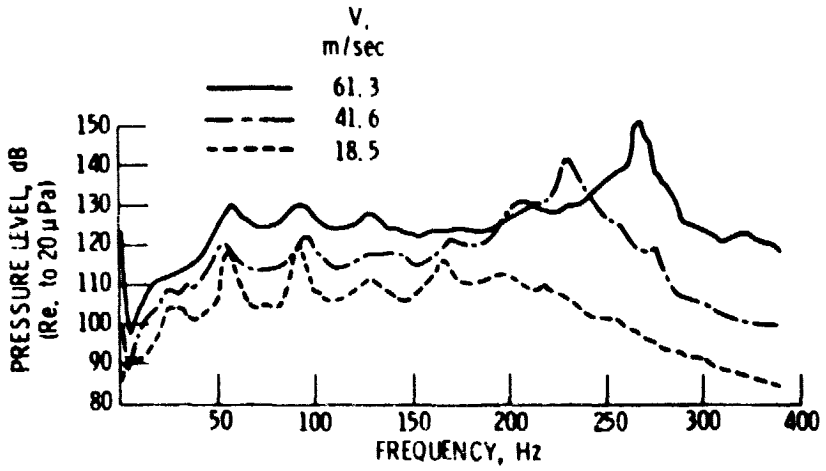

Figure 12. - Pressure auto-spectra measured near exit of long duct.

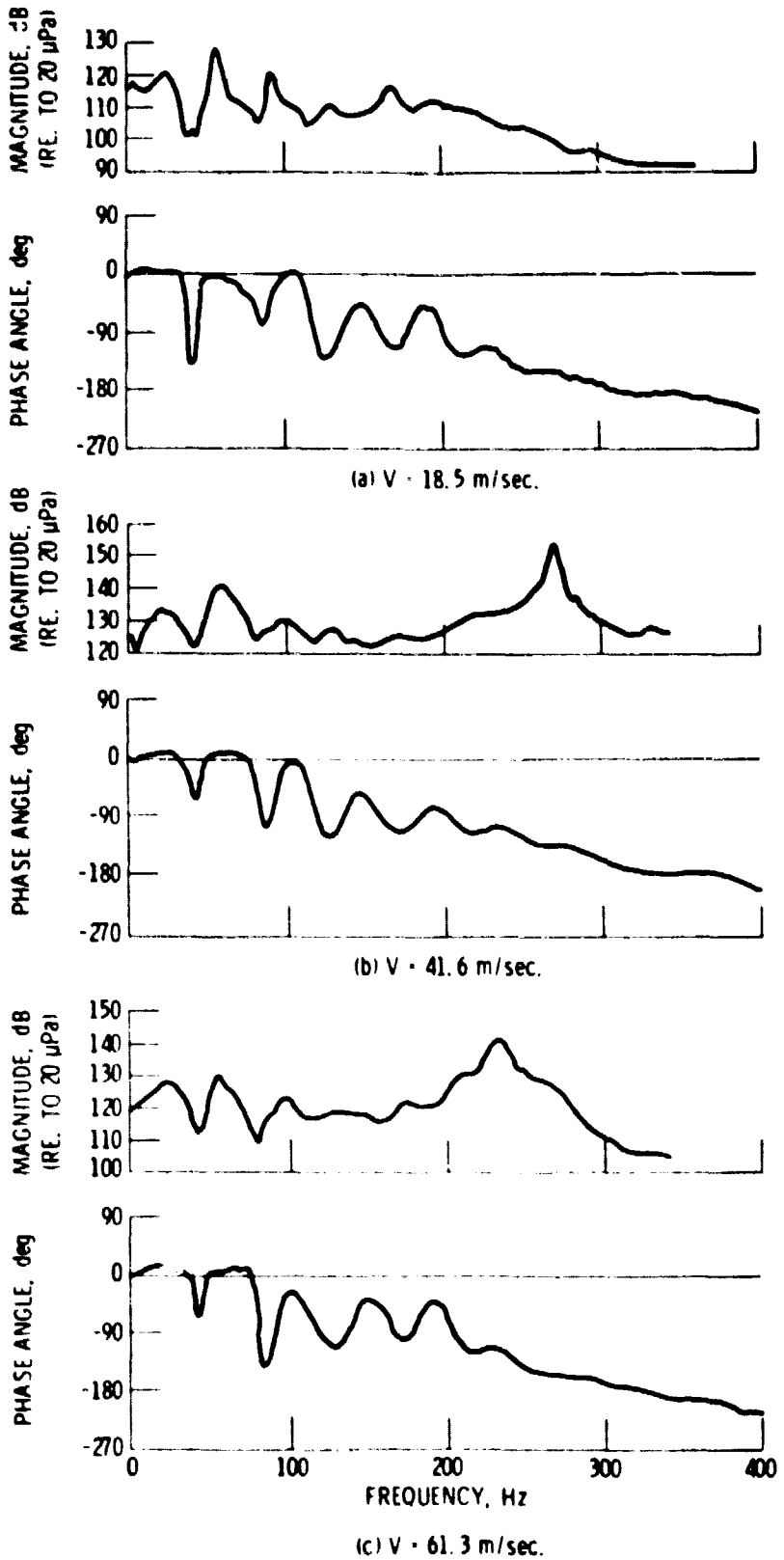

Figure 13. - Pressure cross-spectra measured across area contraction.

due to the presence of waves having approximately equal magnitudes but opposite sign travelling upstream and downstream. Instead the phase plots show both tendencies with the time delay tendency dominating at the higher frequencies.

A large peak appears above 200 Hz in the auto-spectra and cross-spectra measured at air mass flows of 1.13 and 1.68 kg/sec. These peaks appear at such high frequencies that they cannot be related to specific duct resonance harmonics. These peaks may be due to a feedback resonance between the combustor and the duct. They are not analyzed herein.

In the next chapter calculated auto-spectra and cross-spectra will be compared with the measured auto-spectra and cross-spectra discussed in this chapter.

Symbols Used in This Chapter

C_{xy}	real part of cross-spectra
E[ ]	expected value operator
f	frequency
G_x	auto-spectra of x signal
G_y	auto-spectra of y signal
G_{xy}	cross-spectra between x and y signals
i	$(-1)^{1/2}$
PL	pressure level
Q_{xy}	imaginary part of cross-spectra
$X_\theta(f)$	finite Fourier transform of x time signal
$x(\theta)$	x time signal
$Y_\theta(f)$	finite Fourier transform of y time signal
$y(\theta)$	y time signal

Θ	record length, sec
θ	time, sec
ϕ_{xy}	cross-spectrum phase angle

V. COMPARISON WITH EXPERIMENTAL DATA

The single time constant model discussed in Chapter III is used now to calculate auto-spectra and cross-spectra at locations which correspond to the locations of the measured auto-spectra and cross-spectra presented in Chapter IV. The parameters used to calculate the mass fraction and soot particle relaxation time used are given in Table III. The value of the soot particle relaxation time is considered to be 1.5×10^{-6} sec for all cases. The time constant, τ_s/κ_s, used in each example then is due to the presence of different soot particle mass fractions as shown in Table III.

For a wave propagating downstream and for the time constants given in Table III, the sound propagation speed and attenuation calculated by substituting Eq. (3.1.25) into Eq. (2.1.44) and Eq. (2.1.46) are shown in Figure 14. For a time constant of 1.0 sec, the sound propagation speed is 610 m/sec which is the isentropic sound propagation speed. The sound propagation speed is above 600 m/sec above 50 Hz for a time constant of 0.010 sec. However, for a time constant of 0.001 sec, the sound propagation speed varies from the isothermal speed of sound propagation, 510 m/sec, to the isentropic speed of sound at high frequencies. For a time constant of 0.0001 sec the sound propagation speed is the isothermal speed of sound below 340 Hz.

For time constants of 1.0, 0.010, and 0.0001, the attenuation is less than 0.5 dB/m at most frequencies below 340 Hz. However, for a

TABLE III. - Parameters used to calculate dispersion and attenuation due to soot particle-gas heat transfer

t, K	922.0
κ, W/m-k	5.38×10^{-2}
ρ_o, kg/M^3	0.378
c_p, J/kg-K	1100.0
γ	1.4
ρ_s, kg/M^3	1[illegible]0.0
r_s, m	0.342×10^{-6}
c_o, m/sec	609.0
m_s, kg	3.15×10^{-16}
τ_s, sec	1.5×10^{-6}

	Example			
	1 Isothermal	2 Mixed	3 Adiabatic	4 Adiabatic
n, number/m^3	1.8×10^{13}	1.8×10^{12}	1.8×10^{11}	1.8×10^{13}
nm_s, gm/m^3	5.67	0.567	0.0567	5.67×10^{-4}
κ_s, Nm_s/ρ_o	1.5×10^{-2}	1.5×10^{-3}	1.5×10^{-4}	1.5×10^{-6}
τ_s/κ_s, sec	1×10^{-4}	1×10^{-3}	1×10^{-2}	1.0

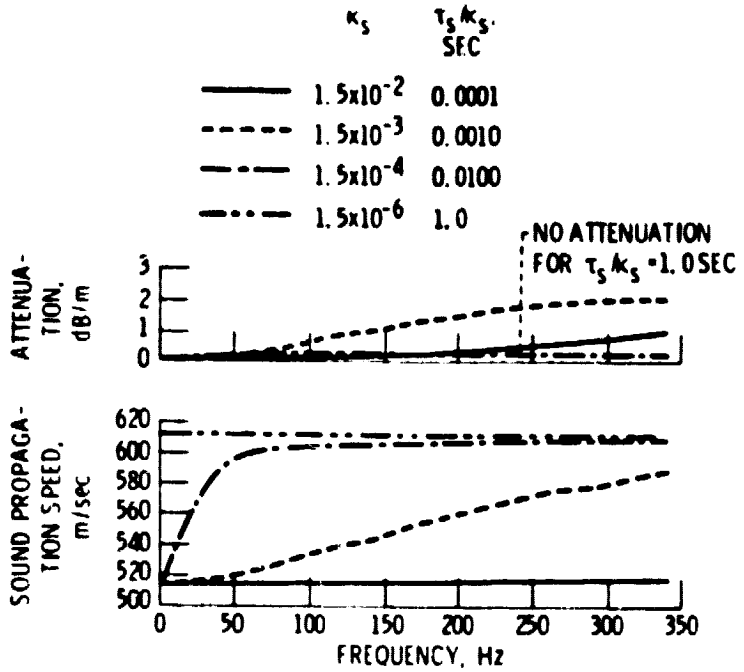

Figure 14. - Calculated attenuation and dispersion.

time constant of 0.001 sec, the attenuation is greater than 1 dB/m over the frequency range of 150 to 340 Hz.

A. Auto-Spectra

Calculated auto-spectra are compared with auto-spectra measured with a mass flow rate of 0.5 kg/sec in Figures 15 to 18. Auto-spectra calculated with τ_s/κ_s = 1.0 sec and 0.001 sec for the location in the spool piece upstream of the area contraction are compared with auto-spectra measured at that location in Figures 15(a) and (b). For τ_s/κ_s = 1.0 sec, the sound propagation speed is isentropic and the attenuation is negligible. Consequently, the dashed curve shown in Figure 15(a) presents the result which would normally be predicted. The calculated dips and peaks shown in Figure 15(a) are in different locations than the ones measured. Also, the dips and peaks are sharp at all frequencies while the measured dips and peaks are sharp only at the low frequencies.

However, for τ_s/κ_s = 0.001 sec, the calculated dips and peaks are in better agreement with the measured dips and peaks. In addition, the dips and peaks are sharp at low frequencies and broad at high frequencies in excellent agreement with the measured spectra. The improvement in the position of the calculated dips and peaks is due to the sound propagation speed calculated with the time constant of 0.001 sec. This time constant produces the nonlinear behavior of the sound propagation speed which compresses the auto-spectra curve shown in Figure 15(a) in a non-linear fashion. Furthermore, the change in time constants from 1.0 to 0.001 sec, changes the spectral structure from having sharp peaks and dips at all frequencies to having sharp peaks and dips at low frequencies and broad peaks and dips at high frequencies.

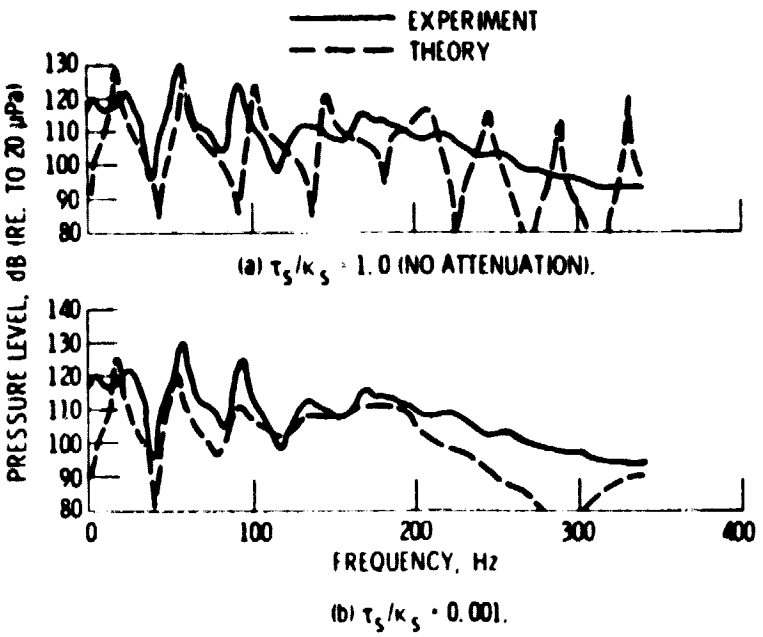

Figure 15. - Comparison of measured and calculated auto-spectra in spool piece (u_0 = 18.5 m/sec).

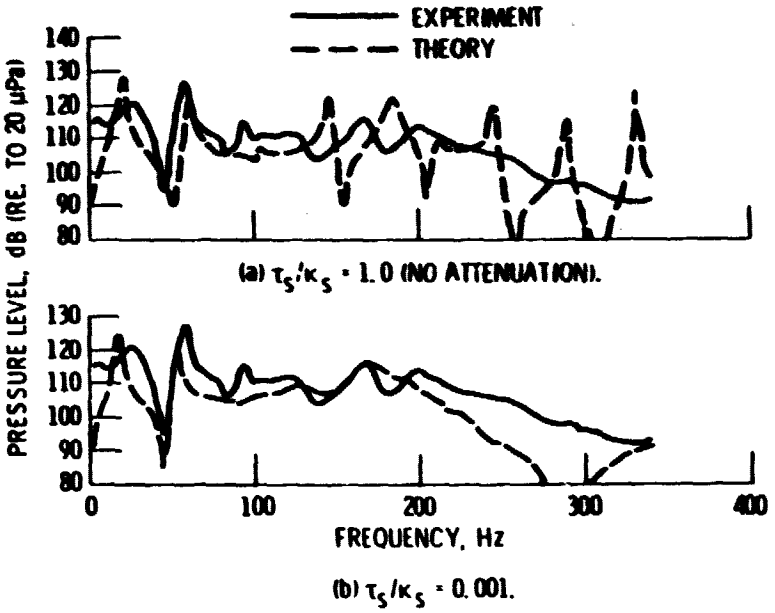

Figure 16. - Comparison of measured and calculated auto-spectra near long duct entrance (u_0 = 18.5 m/sec).

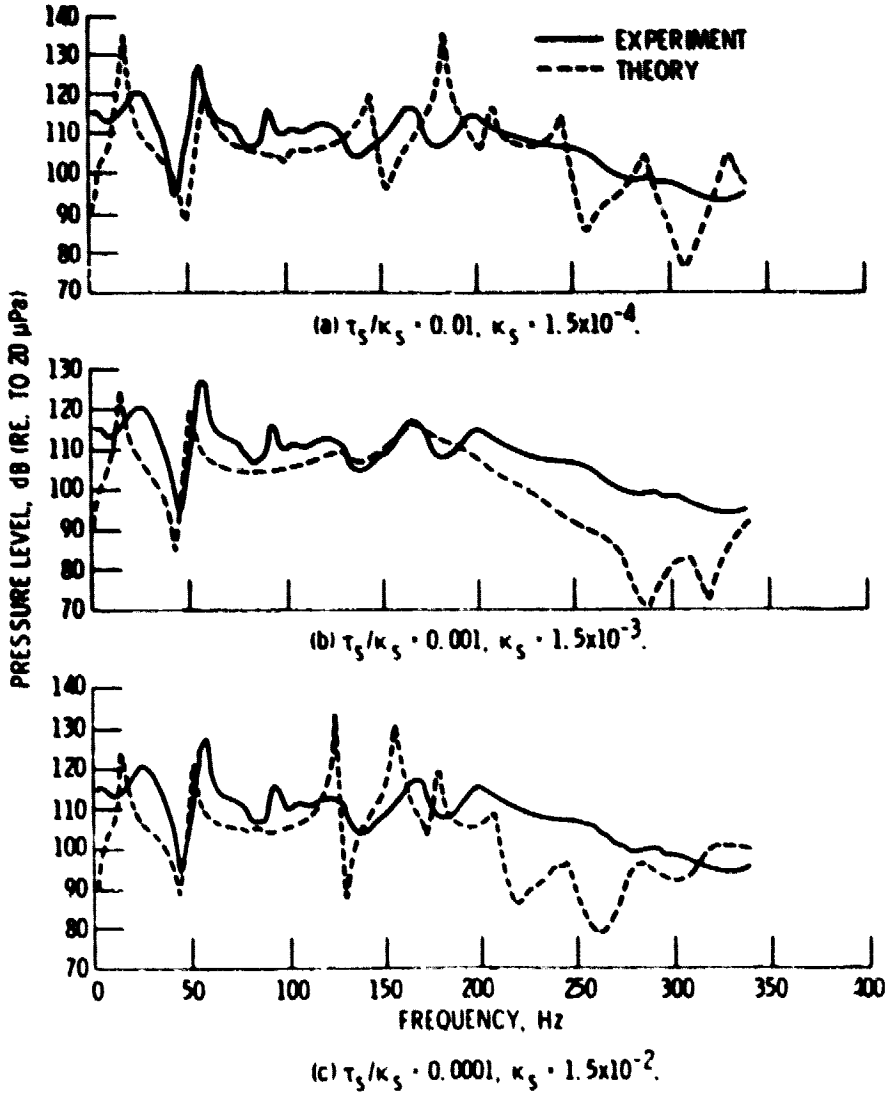

Figure 17. - Comparison of measured and calculated pressure spectra near entrance to long duct (u_0 = 18.5 m/sec).

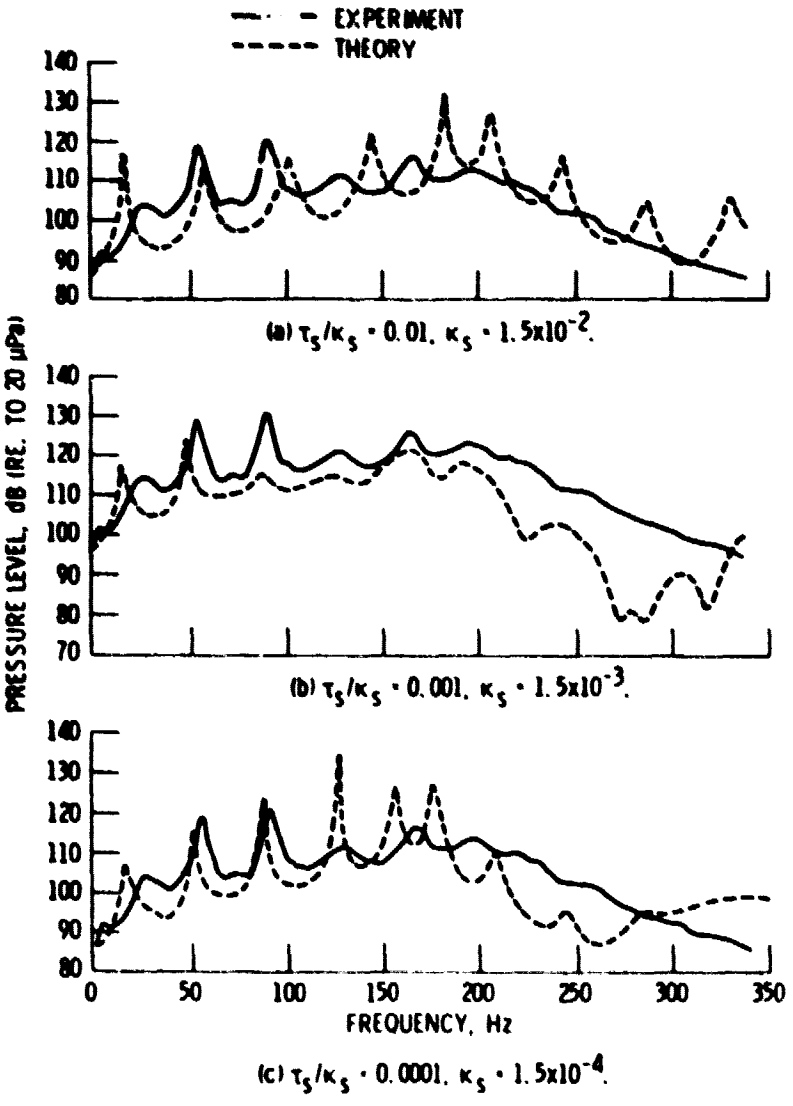

(a) $\tau_s/\kappa_s = 0.01$, $\kappa_s = 1.5 \times 10^{-2}$.

(b) $\tau_s/\kappa_s = 0.001$, $\kappa_s = 1.5 \times 10^{-3}$.

(c) $\tau_s/\kappa_s = 0.0001$, $\kappa_s = 1.5 \times 10^{-4}$.

Figure 18. - Comparison of measured and calculated pressure spectra near exit of long duct ($u_0 = 18.5$ m/sec).

Measured auto-spectra at the location near the long duct entrance downstream of the area contraction are compared with auto-spectra calculated using time constants of 1.0 and 0.001 sec in Figures 16(a) and (b), respectively. Again, calculations made using the 0.001 sec are in better agreement with the measured data.

That using the isothermal speed of sound propagation rather than the isentropic speed of sound propagation in model calculations does not produce auto-spectra which agree with measured auto-spectra is shown in Figures 17 and 18. In these figures measured and calculated spectra near the entrance and near the exit of the long duct are compared. Auto-spectra calculated using a time constant of 0.0001 sec, which produces little attenuation and an isothermal sound propagation speed below 340 Hz, are shown in Figures 17(c) and 18(c). The calculated curves are compressed versions of the curves shown in Figures 17(a) and 18(a) which are calculated with a time constant of 0.01 sec which produces little attenuation and an isentropic sound propagation speed above 80 Hz. Neither the curves calculated with a time constant of 0.01 sec or 0.0001 sec are in as good agreement with the measured data as the curves calculated using a time constant of 0.001 sec shown in Figures 17(b) and 18(b). The changes with mass fraction appear graphically in the form of stretching or as a compression of the basic structure. These changes were easy to recognize but proved difficult to simply explain.

In summary, the single time constant model developed in Chapter III provides a simple, elegant theory which explains the spectral structure of the measured auto-spectra. In addition, the next section shows it also explains the structure of the measured cross-spectra.

B. Cross-Spectra

The cross-spectra calculated using time constants of 1.0 and 0.001 sec are compared with the data measured for u_o = 18 m/sec in Figure 19. The model calculations made using a time constant of 1.0 sec shown in Figure 19(a) produces a cross-spectra which does not look like the measured cross-spectra. However, the cross-spectra calculated using a time constant of 0.001 sec shown in Figure 19(b) does resemble the measured cross-spectra. The peaks and dips in the cross-spectra magnitude calculated using a time constant of 0.001 sec are close to the locations of the peaks and dips in the measured cross-spectra. In addition, the structure of the measured and calculated magnitude curves is similar. Furthermore, the phase angle calculated using a time constant of 0.001 sec and shown in Figure 19(b) is in excellent agreement with the structure of the measured phase angle.

C. Mean Flow

Calculations made using a time constant of 0.001 sec with three different mean flow velocities are shown in Figure 20. The calculated pressure level at the exit of the long duct changes slightly with the mean flow speed at the low frequencies. While the change is greater at the higher frequencies it occurs predominantly in the spectrum level and not in the frequency location of the peaks. Consequently, these changes could not be observed in the measured spectra. However, the measured spectra shown in Figure 11 for the three flow velocities have similar trends at low frequencies. Accordingly, the spectra measured at the higher duct exit flow velocities are also in fair agreement with the model calculations made for the time constant of 0.001 sec.

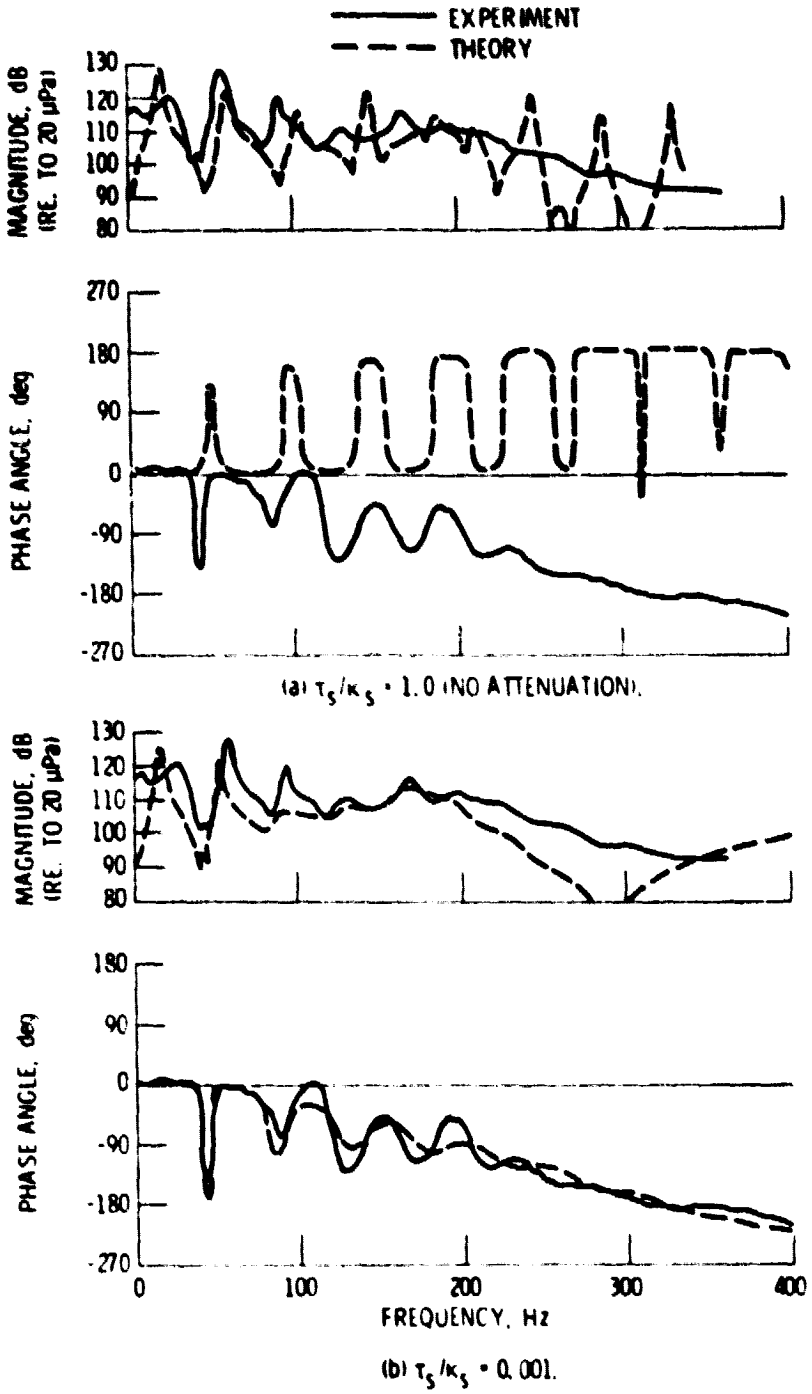

Figure 19. - Comparison of measured and calculated cross-spectrum across area contraction (u_0 = 18.5 m/sec).

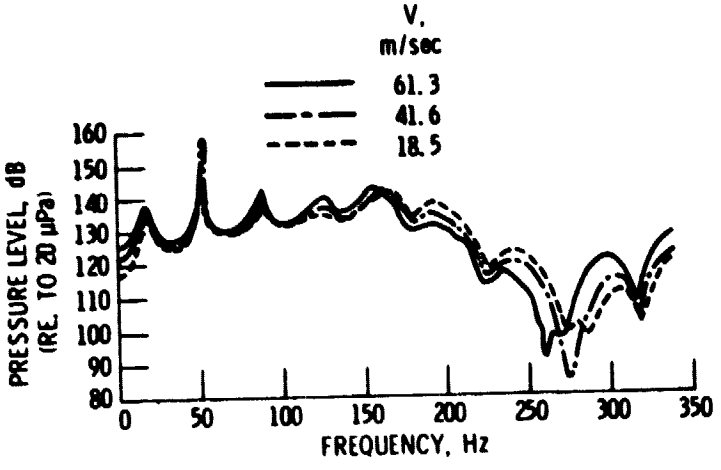

Figure 20. - Effect of flow velocity on computed pressure spectra: τ_s/κ_s = 0.001 sec, $\kappa_s = 1.5 \times 10^{-3}$.

D. Discussion

No attempt was made in this investigation to determine soot particle size or mass concentration. Data in the literature indicate that typical soot particle diameters range from 0.05 to 1 μm (Linden and Heywood (1971)). Smoke concentration ranges from 0.53 to 5.8 gm/m^3 in the primary combustion zone and from 0.00018 to 0.015 gm/m^3 at a combustor exhaust station were found by Norgren (1971). Besides being a function of position in the combustor, smoke concentration was found to be a function of combustor model, fuel-air ratio, and operating pressure by Norgren (1971).

1. Spectra Structure

The spectral structure for a given operating temperature and a given geometry is determined by the value of the ratio of the soot particle thermal relaxation time to the mass fraction. Using Eqs. (2.3.9) and (2.3.12) and the parameters in Table III, the soot particle concentration can be calculated from the soot particle radius for a given value of this time constant by

$$nm_s = 4.84\times10^9\left(r_s^2\right)\Big/\left(\tau_s/\kappa_s\right),\ gm/m^3 \qquad (5.1)$$

This function is plotted in Figure 21 for three values of the time constant. Also shown in Figure 21 is the smoke number for a given soot particle concentration as given by Norgren (1971). The circled point in Figure 21 at $r_s = 0.342$ μm and $(nm_s) = 0.567\ gm/m^3$ corresponds to the value in Table III for $\tau_s/\kappa_s = 0.001$ sec which produced the spectral structure that most resembled the measured structure. This particular point may be unrealistic since it corresponds to a large smoke number. However, any point on the $\tau_s/\kappa_s = 0.001$ sec line would

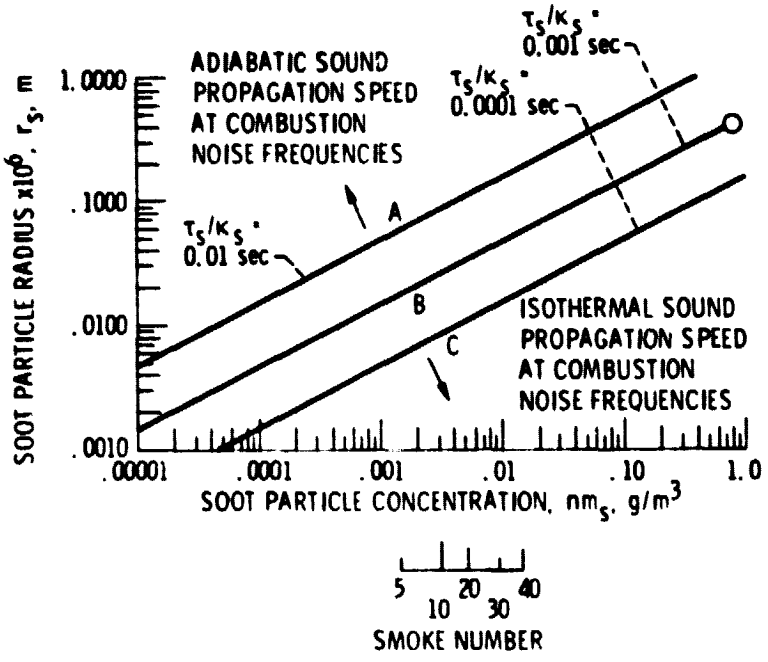

Figure 21. - Parameter map for τ_s/κ_s.

also produce the same spectral structure. Consequently, these results, to this extent, are independent of the parameter in Table III. Unfortunately, this also means that the method cannot independently be used to estimate the soot particle radius or mass concentration.

Figure 21 also indicates how the sound propagation speed varies with soot particle radius and mass concentration at combustion noise frequencies. The sound propagation speed can be determined from Eqs. (2.1.44) and (3.1.25) to (3.1.28). The sound propagation speed is isothermal at frequencies for which $(\omega\tau_s/\kappa_s)$ is less than unity. Consequently, sound propagates isothermally at frequencies less than a corner or break frequency, f, given by

$$f_b = \frac{1}{2\pi(\tau_s/\kappa_s)} \tag{5.2}$$

Above the corner or break frequency the sound propagation speed is changing from isothermal to isentropic. Along curves A, B, and C the break frequencies are, respectively, 15.91, 159.1, and 1591 Hz. For a time constant of 0.01 sec, corresponding to curve A in Figure 21, the speed of sound propagation exhibited in Figure 14 is less than 540 m/sec at frequencies below 15.91 Hz. Also, for a time constant of 0.001 sec, corresponding to curve B in Figure 21, the speed of sound propagation exhibited in Figure 14 is less than 540 m/sec at frequencies below 159.1 Hz. Consequently, at combustion noise frequencies, in the region above curve A in Figure 21 the sound propagation speed calculated is isentropic. In the region below curve C the calculated speed of sound is isothermal. However, along curve B a mixed speed of sound propagation occurs at combustion noise frequencies.

The maximum amount of attenuation is difficult to determine from Eq. (2.1.46). However, it is possible to determine the frequency which maximizes the phase angle of $(ik\Omega_o)$. The attenuation at this frequency is about 54 percent of the maximum attenuation. Substituting Eq. (3.1.25) into Eq. (2.1.46) and maximizing the phase angle shows the phase angle maximum attenuation at any operating temperature, for M = 0.0, occurs at

$$f_{max} = \frac{\gamma^{1/2}}{2\pi(\tau_s/\kappa_s)} \tag{5.3}$$

The phase angle maximum attenuation at this frequency is

$$\alpha_{max} = 4.96 \frac{f_{max}}{c_o}, \text{ dB/m} \tag{5.4}$$

Thus, along curves A, B, and C in Figure 21, the phase angle maximum attenuation occurs, respectively, at 18.83, 188.3, and 1883 Hz and is, respectively, 0.15, 1.53, and 15.3 dB/m. The attenuation is, respectively, 0.2846, 2.846, and 28.46 dB/m at $f = 1.0\times10^{99}$.

The measured spectra shown in Figures 10, 11, and 12 may have similar structure at each operating condition because the value of the ratio of the heat transfer time constant to mass fraction did not change much with operating condition and was approximately 0.001 sec.

On the other hand, if the broad peak above 200 Hz, which occurs in the measured spectra taken with long duct flow velocities of 41.6 and 61.3 m/sec, is due to feedback between the duct acoustics and the combustion process, then its occurrence at these operating conditions may be due to a decrease in acoustic damping of the longitudinal waves due to a change in soot mass fraction or radius at these operating

conditions. This possibility suggests that soot particles can be used to control certain types of combustor instability by attenuating pressure oscillations at critical frequencies.

2. Model Assumptions

In Chapter III the soot particles are assumed to have a uniform temperature and no mass loss because these simple assumptions produced theoretical results which agreed with measurements, because they greatly simplified the analysis and because more complicated assumptions did not produce better models. The actual effect of a pressure perturbation on the temperature and mass equilibrium between a liquid or solid particle and a gas is a complex problem depending on at least the following influences:

1. Convective heat transfer to or from the particle.
2. Heat transfer within the particle.
3. Mass transfer to or from the particle.
4. Surface chemical reactions on a soot particle.
5. Liquid-vapor phase transitions of a droplet.
6. Radiative heat transfer.

Radiative heat transfer is not an important factor in this case because the combustion duct operating temperatures are low.

Many models can be constructed which describe this problem for a soot particle. As an example, it is possible to analyze this problem by assuming instantaneous heat transfer within the particle and by using a pressure and temperature dependent surface chemical reaction which effect heat and mass transfer as was done in Chapter II. This model is complex and depends on many parameters.

In Chapter III the particles are assumed to have a uniform temperature. This is assumed to be due to some unspecified pressure and temperature dependent surface chemical reaction. The model developed is dependent on only a single parameter, the ratio of τ_s to κ_s.

It is possible to analyze this problem by ignoring surface chemical reaction effects on heat and mass transfer and by assuming instantaneous heat transfer within the particle. The resulting thermal relaxation time for a 1-μm particle is about 0.3 μsec which shows that this type of particle quickly follows any temperature change and does not have a constant time independent temperature. However, experiments show that smoke concentrations of soot particles are reduced as soot travels from a measuring station at the primary combustion zone to one at the combustor exhaust (Norgren (1971)). Consequently, surface chemical reactions cannot be ignored. Further study is needed to discover what assumptions are best for analyzing this problem.

Symbols Used in This Chapter

f_b corner or break frequency, Hz

f_{max} frequency of phase angle maximum, Hz

α_{max} phase angle maximum attenuation, dB/m

VI. SUMMARY AND CONCLUDING REMARKS

A. Summary

In Chapter I, the motivation for the combined experimental and analytical program described in this dissertation is established. Specifically, the importance of combustion noise in future aircraft design is indicated. Current approaches to combustion noise research are discussed. Next, the need to study the propagation of combustion noise is established. Then the topics investigated herein are specified as being concerned with answering the following two questions:

(1) What is the wave equation in an operating ducted combustion system?

(2) What formulation of the solution to the wave equation provides an acceptable mathematical model of an operating ducted combustion system?

Finally, the available work of interest in these areas is discussed.

In Chapter II, the plane wave equation as modified for the response of a fuel droplet cloud or a soot particle cloud is discussed. It is shown that at low frequencies sound can propagate at speeds near the isothermal speed of sound.

In Chapter III, an acoustic model of the combustion duct system which depends on a single time constant is presented. This chapter describes the use of a two-port transmission line using transfer matrices to represent sound propagation in the homogeneous differential equation solution region of an operating ducted combustion system. The

use of an approach based on construction of the one-dimensional Green's function in the non-homogeneous region is discussed.

Chapter IV first describes the experimental hardware, instrumentation, and frequency domain representation. Next, measured auto-spectra and cross-spectra are presented. Briefly, the ducted combustion system consisted of a J-47 can combustor, followed by a short spool piece, and then by a long duct. Fluctuating pressure measurements within the operating ducted combustion system were made with specially constructed "semi-infinite" waveguide probes, with conventional microphones being used as the pressure transducers. The data obtained from these probes were off-line processed on a fast Fourier transform digital signal processor. The processor was used to obtain pressure level spectra as well as cross-spectra between internal pressure measurements.

In Chapter V the measured auto-spectra and cross-spectra are compared with the calculated auto-spectra and cross-spectra and the results are discussed. Auto-spectra and cross-spectra calculated using a time constant of 0.001 sec in the model developed in Chapter III are in excellent agreement with the measured auto-spectra and cross-spectra.

B. Recommendations for Future Work

The experimental data obtained in the present study support the idea that combustor emissions in the duct act as the primary mechanism producing the attenuation and dispersion of combustion noise in this operating liquid fuel combustion system. However, combined acoustic and combustion measurements need to be made if the theory is to be compared with the experimental data. Thus, this is an area

where continuing research efforts should be directed. Unfortunately, answers to the many remaining questions will probably be found only through multidisciplinary research.

C. Concluding Remarks

The usefulness of a single parameter linear system model to describe the dynamic behavior of an operating ducted liquid fuel combustion system has been established. When allowance is made for dispersion and attenuation effects and the boundary conditions are properly specified good agreement between measured and analytical spectra and cross-spectra is achieved. However, it is not clear if these results can be related or applied to actual engines. For example, the design of liners or suppressors for combustion noise reduction obviously requires knowledge of the appropriate wave equation and the correct propagation speed of sound. Clearly, if dispersion and attenuation due to soot particles or liquid fuel droplets occurs in actual engines at low frequencies it must be taken into account. However, the propagation speed of sound at low frequencies in actual engines is unknown.

Finally, as stated in the INTRODUCTION, the objective was to use a dynamic system state-space approach to study the operating ducted combustion system. The measurement techniques described herein, as well as these mathematical methods have been available for many years. It is the bringing together of both in a unified research program in a new area with practical objectives that lead to this work making a major contribution to the study of combustion noise.

APPENDIX A

RESPONSE OF THE FUEL DROPLET CLOUD

The purpose of this appendix is to discuss the derivation of the transfer functions $\mathcal{M}(\omega)/\rho_o$ and $\mathcal{J}(\omega)/c_p$ for the case of sound propagation in a liquid fuel droplet cloud following the approach used by Marble and Candel (1975) for sound propagation in a water droplet cloud.

The following assumptions are made:

1. The fuel drop is spherically symmetric.

2. Convection corrections can be obtained with experimental correlations.

3. Fluid properties are assumed constant with the property values determined at an appropriate reference condition. The liquid fuel is assumed to be a single pure component.

4. The relationship between the gas phase fuel concentration and liquid fuel droplet temperature is given by the vapor pressure correlation for the pure liquid, i.e., the Clausius-Clapeyron equation.

5. The ambient gases have negligible solubility in the liquid phase and only the fuel vapor is diffusing from the surface.

6. The radial motion of the liquid surface is assumed to be small.

7. Heat transfer by radiation is neglected.

8. Mass diffusion is represented by an effective binary diffusion law corrected for convection, and the Dufour effect is neglected in the heat flux (Bird, Stewart, and Lightfoot (1960), and Welty, Wicks, and Wilson (1969)). The diffusion coefficient is calculated from

$$D_{AB} = 1.8583\times10^{-7} \sqrt{t^3 \left(\frac{1}{(MW)_A} + \frac{1}{(MW)_B}\right)} \Big/ p\sigma_{AB}^2, \ m^2/sec \qquad (A\text{-}1)$$

and the diffusion Nusselt number is given by

$$Nu_D = 2 + 6\ Re^{1/2} Sc^{1/3} \qquad (A\text{-}2)$$

9. Reaction effects such as fuel oxidation are negligible.

10. Heat transfer is calculated using the Chapman-Ensog formula for the thermal conductivity of a monatomic gas at low density at temperature t corrected for convection (Bird, Stewart, and Lightfoot (1960), and Welty, Wicks, and Wilson (1969)). The thermal conductivity is calculated from

$$\kappa = 8.3224\times10^{-2} \sqrt{\frac{t}{(MW)}} \Big/ \sigma^2 \Omega_k, \ watt/mK \qquad (A\text{-}3)$$

and the heat transfer Nusselt number is given by

$$Nu_H = 2 + 6\ Re^{1/2} Pr^{1/3} \qquad (A\text{-}4)$$

Surface tension and surface charge corrections are omitted.

11. The fluid in the drops is rapidly mixing creating droplets of uniform temperature.

12. The mean flow velocity is neglected in the vapor and bulk gas continuity equations.

A perturbation in pressure causes a perturbation in the bulk gas temperature, $t_{\infty,1}$, the fuel droplet temperature, t_p, the mass source, ϕ_1, and the partial pressure of the fuel far from the drop, $p_{v,\infty,1}$. The following system of equations is derived to relate these perturbations. This common factor is dropped henceforth.

The bulk gas energy equation will be considered first. Since the heat conducted from n liquid fuel droplets of radius r_L into a unit volume of gas having thermal conductivity κ by a convective heat transfer process with Nusselt number Nu_H is equal to the product of temperature and the rate of entropy rise, the bulk gas energy equation is

$$t_o \rho_o \frac{ds_1}{d\theta} = n\left(4\pi r_L^2\right) \frac{Nu_H}{d_L} \kappa (t_{V-L,1} - t_{\infty,1}) \tag{A-5}$$

This can be written as

$$\frac{d}{d\theta}\left(\frac{s_1}{c_p}\right) = \frac{\kappa_L}{\tau_L}\left(\frac{t_{V-L,1} - t_{\infty,1}}{t_o}\right) \tag{A-6}$$

where the fuel droplet mass loading is given by nm_L, the fuel droplet mass fraction, κ_L, is

$$\kappa_L = nm_L/\rho_o \tag{A-7}$$

and the fuel droplet thermal relaxation time, τ_L, is

$$\tau_L = m_L c_p / [4\pi r_L \kappa (Nu_H/2)] \tag{A-8}$$

Perturbations in bulk gas temperature and pressure are related to perturbations of fuel droplet temperature next. A small perturbation expansion of the perfect gas state equation (Eq. (2.1.5)) yields

$$\rho_1/\rho_o = p_1/p_o - t_{\infty,1}/t_o \tag{A-9}$$

Equation (A-9) is then substituted into the zero mean flow, small perturbation form of the ideal gas entropy equation (Eq. (2.1.8)) to eliminate the density perturbation. Finally, the time derivative is taken and the bulk gas energy equation (Eq. (A-6)) is used with the result that

$$\frac{d}{d\theta}\left[\frac{p_1}{\gamma p_o} - \frac{\rho_1}{\rho_o}\right] = \frac{d}{d\theta}\left[\frac{(1-\gamma)}{\gamma}\frac{p_1}{p_o} + \frac{t_{\infty,1}}{t_o}\right] = \frac{d}{d\theta}\left(\frac{s}{c_p}\right) = \frac{\kappa_L}{\tau_L}\left(\frac{t_{V-L,1} - t_{\infty,1}}{t_o}\right) \tag{A-10}$$

or in terms of the liquid mass fraction and thermal time delay

$$\frac{d}{d\theta}\left(\frac{t_{\infty,1}}{t_o}\right) - (\gamma - 1)\frac{d}{d\theta}\left(\frac{p_1}{\gamma p_o}\right) = \frac{\kappa_L}{\tau_L}\left(\frac{t_{V-L,1} - t_{\infty,1}}{t_o}\right) \tag{A-11}$$

The discussion so far has neglected the mass source term, ϕ_1. The first step in introducing this term is to relate perturbations in vapor pressure, fuel droplet temperature, and mass flux to pressure perturbations. The time rate of change of the droplet mass is governed by the rate at which the fuel vapor can diffuse into the background gas. Thus,

$$\frac{d}{d\theta}\left(\frac{4}{3}\pi r_L^3 \rho_L\right) = 4\pi r_L^2 \rho_o \frac{D_{Vg}}{d_L} Nu_D \left(\frac{Y_{V-L} - Y_{V,\infty}}{1 - Y_{V-L}}\right) = \frac{\phi}{n} \tag{A-12}$$

The mass of vapor entering a unit volume occupied by n droplets is in terms of the partial pressure

$$\phi = n 4\pi r_L \rho_o D_{Vg} \frac{Nu_D}{2}\left[\frac{p_{V-L} - p_{V,\infty}}{p_o - p_{V-L}}\right] \tag{A-13}$$

For a small vapor pressure perturbation

$$p = p_o + p_1 \tag{A-14}$$

a small mass addition occurs

$$\phi = \phi_o + \phi_1 \tag{A-15}$$

where

$$\phi_1 = n4\pi r_L \rho_o D_{Vg} \left(\frac{Nu_D}{2}\right) \left(\frac{p_{V-L,1} - p_{V,\infty,1}}{p_o}\right) \tag{A-16}$$

The Clausius-Clapeyron equation is used to relate the fuel vapor pressure perturbation to the fuel droplet temperature perturbation as follows:

$$\bar{t}_{V-L} = t_o + t_{V-L,1} \tag{A-17}$$

$$\frac{p_{V-L,1}}{t_{V-L,1}} = \frac{H_{V-L}}{t_o(1/\rho_g - 1/\rho_f)} = \frac{H_{V-L}}{t_c} \frac{(MW)_V p_{V,o}}{\mathcal{R} p_o} \tag{A-18}$$

since

$$1/\rho_g >> 1/\rho_f \tag{A-19}$$

and

$$p_{V,o} = \rho_V \frac{\mathcal{R} t_o}{(MW)_V} \tag{A-20}$$

Substituting Eqs. (A-17) and (A-18) into Eq. (A-16) yields

$$\phi_1 = n4\pi r_L \rho D_{Vg} \left(\frac{Nu_D}{2}\right) \left[\frac{H_{LV}(MW)_V}{\mathcal{R} t_o} \frac{p_{V,o}}{p_o} \frac{t_{L,1}}{t_o} - \frac{p_{V,\infty,1}}{p_o}\right] \tag{A-21}$$

Now, with the following thermodynamic relations:

$$c_p - c_V = \mathcal{R}/(MW)_g \tag{A-22}$$

$$\gamma = c_p/c_V \tag{A-23}$$

$$\gamma - 1 = \frac{\mathcal{R}}{(MW)_g c_V} = \frac{\gamma \mathcal{R}}{(MW)_g c_p} \tag{A-24}$$

Eq. (A-21) can be written as

$$\frac{\phi_1}{\rho_o} = \left(\frac{nm_L}{\rho_o}\right)\left[\frac{4\pi r_L \rho_o}{m} D_{Vg}\left(\frac{Nu_D}{2}\right)\right]\frac{p_{V,o}}{p_o}\left[\left(\frac{H_{V-L}}{t_o c_p}\right)\left(\frac{\gamma}{\gamma - 1}\right)\frac{(MW)_V}{(MW)_g}\frac{t_{L,1}}{t_o} - \frac{p_{V,\infty,1}}{p_{V,o}}\right] \tag{A-25}$$

or as

$$\frac{\phi_1}{\rho_o} = \frac{\kappa_p}{\tau_D} Y_V\left[\beta \frac{\gamma}{\gamma - 1}\eta \frac{t_{L,1}}{t_o} - \frac{p_{V,\infty,1}}{p_{V,o}}\right] \tag{A-26}$$

where the fuel droplet mass fraction, κ_L, is again given by

$$\kappa_L = nm/\rho_o \tag{A-27}$$

the molecular weight ratio of vapor-to-bulk gas, β, is given by

$$\beta = \frac{(MW)_V}{(MW)_g} \tag{A-28}$$

the latent heat parameter, η, is given by

$$\eta = \frac{H_{V-L}}{t_o c_p} \tag{A-29}$$

and the diffusion relaxation time, τ_D, is given by

$$\tau_D = \frac{m_L}{\left[4\pi r_L \rho_o D_{Vg}\left(\frac{Nu_D}{2}\right)\right]} \tag{A-30}$$

The fuel droplet energy equation involves the mass flux perturbation as follows. The time rate of change of a fuel droplets energy is equal to the instantaneous difference between the convective heat input and the heat required for surface vaporization. Thus,

$$\frac{d}{d\theta}\left[\left(\frac{4}{3}\pi r_L^3\right)\rho_L c_L t_{V-L,1}\right] = \frac{d}{d\theta}[m_L c_L t_{V-L,1}]$$

$$= -4\pi r_L^2\left(\frac{Nu_H}{d_L}\right)\kappa(t_{V-L} - t_{\infty,1}) - H_{LV}\frac{d}{d\theta}\left(\frac{4}{3}\pi r_L^3 \rho_L\right) \tag{A-31}$$

or

$$K_L\left(\frac{c_L}{c_p}\right)\frac{d}{d\theta}\left(\frac{t_{V-L,1}}{t_o}\right) = -\frac{\kappa_p}{\tau_{T,L}}\left(\frac{t_{V-L,1} - t_{\infty,1}}{t_o}\right) - \eta\frac{\phi}{\rho_o} \tag{A-32}$$

where

$$\tau_{T,L} = \frac{m_L c_p}{4\pi r^2\left(\frac{Nu_H}{d_L}\right)\kappa} \tag{A-33}$$

The fuel vapor mass source perturbation is related to the fuel partial pressure perturbation and the total pressure perturbation as follows. From the vapor continuity equation

$$\frac{\partial}{\partial\theta}\rho_{V,1} + \rho_{V,o}\frac{\partial u_1}{\partial x} = \phi_1 \tag{A-34}$$

and from the bulk gas continuity equation

$$\frac{\partial}{\partial \theta} \rho_1 + \rho_o \frac{\partial u_1}{\partial x} = \phi_1 \tag{A-35}$$

Using Eqs. (A-34) and (A-35), the velocity gradient can be eliminated as follows:

$$\frac{\partial u_1}{\partial x} = \frac{\phi_1}{\rho_{V,o}} - \frac{1}{\rho_{V,o}} \frac{\partial \rho_{V,1}}{\partial \theta} = \frac{\phi_1}{\rho_o} - \frac{1}{\rho_o} \frac{\partial \rho_1}{\partial \theta} \tag{A-36}$$

Thus,

$$\phi \left[\frac{1}{\rho_{V,o}} - \frac{1}{\rho_o} \right] = \left(\frac{1}{\rho_{V,o}} \right) \frac{\partial \rho_{V,1}}{\partial \theta} - \left(\frac{1}{\rho_o} \right) \frac{\partial \rho_1}{\partial \theta} \tag{A-37}$$

Since the vapor partial pressure can be calculated from the gas law

$$p_{V,\infty} = \frac{\mathcal{R}_V}{(MR)_V} t_o \rho_V \tag{A-38}$$

and the vapor partial pressure ratio, Y_V, is

$$Y_V = \frac{p_{V,\infty}}{p_o} = \frac{\rho_{V,o}}{\rho_o} \tag{A-39}$$

it follows that:

$$\frac{\phi_1}{\rho_o} \left[\frac{1 - Y_V}{\gamma Y_V} \right] = \frac{\partial}{\partial \theta} \left[\frac{p_{V,\infty,1}}{\gamma p_{V,o}} - \frac{p_1}{\gamma p_o} \right] \tag{A-40}$$

The Fourier transforms of Eqs. (A-26), (A-11), (A-32), and (A-40) can be written in matrix form as

$$\mathcal{A}\vec{Y}_1 = \mathcal{A}\begin{bmatrix} \frac{t_{=,1}}{t_o} \\ \frac{t_{V-L,1}}{t_o} \\ \frac{\phi_1}{\rho_o} \\ \frac{p_{V,=,1}}{p_{V,o}} \end{bmatrix} = \begin{bmatrix} 0 \\ (-i\omega)(\gamma - 1) \\ 0 \\ (-i\omega) \end{bmatrix} \phi\left[\frac{p_1}{\gamma p_o}\right] = \vec{U} \qquad \text{(A-41)}$$

where

$$\mathcal{A} = \begin{bmatrix} 0 & -\frac{\kappa_p}{\tau_D} Y_V \frac{\beta\gamma}{\gamma - 1} n & 1 & \frac{\kappa_p Y_V}{\tau_D} \\ \left(-i\omega + \frac{\kappa_p}{\tau_{T,L}}\right) & -\frac{\kappa_p}{\tau_{T,L}} & 0 & 0 \\ -\frac{\kappa_p}{\tau_{T,L}} & \left[\kappa_p \frac{c_L}{c_p}(-i\omega) + \frac{\kappa_p}{\tau_{T,L}}\right] & n & 0 \\ 0 & 0 & -\left[\frac{1 - Y_V}{\gamma Y_V}\right] & \left(-\frac{i\omega}{\gamma}\right) \end{bmatrix}$$

(A-42)

$\vec{Y}$ is the system state vector and $\vec{U}$ is the system forcing function.

The solution is then

$$\vec{Y}_1 = \mathcal{A}^{-1}\vec{U} \qquad \text{(A-43)}$$

After solving Eq. (A-43), the entropy source transfer function is found using Eq. (A-10)

$$\mathcal{F}\left[\frac{s}{c_p}\right] = \frac{1}{(-i\omega)}\left[\frac{\kappa_L}{\tau_{TL}}\right]\left\{\mathcal{F}\left[\frac{t_{V-L,1}}{t_o}\right] - \mathcal{F}\left[\frac{t_{-,1}}{t_o}\right]\right\} = \frac{\mathcal{J}(\omega)}{c_p}\,\mathcal{F}\left[\frac{p_1}{\gamma p_o}\right] \qquad \text{(A-44)}$$

and the mass source transfer function is found using Eq. (2.1.8).

Symbols Used in This Appendix

$\mathcal{A}$	matrix
c_L	specific heat of liquid fuel
c_p	gas specific heat at constant pressure
D_{AB}	mass diffusivity of A through B
d_L	diameter, m
H	enthalpy
i	$(-1)^{1/2}$
(MW)	molecular weight
m_L	liquid fuel droplet mass, kg
Nu_H	heat transfer Nusselt number, hd/κ_L
Nu_D	mass transfer Nusselt number, kg/D_{AB}
n	number of particles per unit volume
p	pressure, N/m
Pr	Prandtl number, $\mu cp/\kappa$
$\mathcal{R}$	gas constant
Re	Reynolds number, du/μ
r	radius, m
$\mathcal{J}(\omega)$	transfer function for response of entropy source to a pressure perturbation
Sc	Schmidt number, μ/D_{AB}

s	entropy of gas, J/kg-K
t	temperature, K
$\vec{U}$	system forcing function
u	speed, m/sec
x	Cartesian coordinate
$\vec{Y}$	system state vector
Y	relative concentration, partial pressure ratio or density ratio
β	molecular weight ratio of vapor to gas
γ	ratio of specific heat at constant pressure to specific heat at constant volume
η	latent heat parameter, $H_{LV}/t_o c_p$
κ	gas thermal conductivity
κ_L	liquid droplet mass fraction, nm_L/ρ_o
θ	time, sec
μ	gas viscosity
ρ	density, kg/m^3
$\sigma_{A,B}$	collision diameter a Lennard-Jones parameter, A
τ_D	diffusion relaxation time, sec
τ_{TL}	liquid droplet thermal relaxation time, sec
ϕ	mass source rate
Ω_K	collision integral based on Lennard-Jones Potential
ω	angular frequency, radians/sec

Subscripts:

D	diffusion
H	heat transfer

L	liquid
V	fuel vapor
V-L	fuel vapor - liquid fuel
Vg	fuel vap - air
o	mean value
1	perturbed value
∞	far from soot particle or droplet

APPENDIX B

SPECTRUM FUNCTION CONFIDENCE LIMITS

The purpose of this appendix is to discuss some of the statistical and computational considerations involved in the random data analysis reported herein. The primary source for this material is Bendat and Piersol (1971).

The digital signal processor performing the random data analysis discussed herein digitized each sample record of data into 1024 words at a sampling rate, f_s, 2.048 times the highest frequency selected for analysis, f_m. Accordingly, the processor memory period or sample record length is

$$T = \left(\frac{\text{Number of words}}{\text{Record}}\right)\left(\frac{1}{\text{Number of words/sec}}\right) = \frac{1024}{2.048\ f_m} = \frac{500}{f_m},\ \frac{\text{sec}}{\text{Record}}$$

The resolution bandwidth is

$$B_e = \frac{1}{T} = \frac{f_m}{500}$$

Next, the finite Fourier transform is taken to obtain a single estimate of the power spectral density function

$$\hat{G}_x(f) = \frac{2}{T}\,|X(f,T)|^2$$

where

$$X(f,T) = \int_0^T X(\theta)e^{-i2\pi f\theta}\, d\theta = X_R(f,T) + iX_I(f,T)$$

and

$$|X(f,T)|^2 = X_R^2(f,T) + X_I^2(f,T)$$

The sample distribution of $\hat{G}_x(f,T)$ is determined as follows. Assuming $X(t)$ is a Gaussian random variable, then $X_R(f,T)$ and $X_I(f,T)$ are Gaussian uncorrelated random variables with zero mean and equal variances since the Fourier transform is a linear operation. Consequently, the quantity

$$|X(f,t)|^2 = X_R^2(f,T) + X_I^2(f,T)$$

is the sum of the square of two independent Guassian variables. Thus, each frequency component of the estimate $G(f,T)$ will have a sampling distribution

$$\frac{G(f,T)}{G(f)} = \frac{\chi_2^2}{2}$$

where χ_2^2 is the chi-square variable with $n = 2$ degrees of freedom.

The $(1 - \alpha)$ confidence interval for the single record is

$$\left[\frac{2\tilde{G}(f)}{\chi_2^2(\alpha/2)} < G(f) < \frac{2\tilde{G}(f)}{\chi_2^2(1 - \alpha/2)}\right]$$

The $(1 - \alpha)$ confidence interval expressed in terms of decibels is

$$\left[10 \log_{10}\hat{G}(f) + 10 \log_{10}\left[\frac{2}{\chi^2_2(\alpha/2)}\right] < 10 \log_{10}G(f) < 10 \log_{10}\hat{G}(f) + 10 \log_{10}\left[\frac{2}{\chi^2_2(1 - \alpha/2)}\right]\right]$$

For a 99-percent confidence interval

$$\chi^2_2(\alpha/2) = \chi^2(0.005) = 10.597$$

$$\chi^2_2(1 - \alpha/2) = \chi^2(0.995)0.01$$

Thus

$$\left[10 \log_{10}\hat{G}(f) + 10 \log_{10}\frac{2}{10.597} < 10 \log_{10}G(f) < 10 \log_{10}\hat{G}(f) + 10 \log_{10}\frac{2}{0.01}\right]$$

or

$$\left[10 \log_{10}\hat{G}(f) - 7.2 \text{ dB} < 10 \log_{10}G(f) < 10 \log_{10}\hat{G}(f) + 23 \text{ dB}\right]$$

The error for a single estimate is unacceptable. The error is reduced by averaging over an ensemble of estimates. This is done by computing N disjoint, that is, independent, sample records and averaging the N estimates at each frequency of spectral component.

The total number of degrees of freedom becomes

$$n = 2N$$

For a total tape record of 120 seconds, the maximum number of independent sample records is

$$N = 120/T$$

For the computation reported herein:

$$f_m = 1000 \text{ Hz}$$

$$f_s = 2048 \text{ Hz}$$

$$T = 1/2 \text{ sec}$$

$$\Delta = 2 \text{ Hz}$$

$$N = 240$$

However, due to the processor design and the use of redundant data the number of independent samples was less than 240 but more than 128. For the following calculations $N = 128$ is used. Thus

$$n = 256$$

For n greater than 30, a normal approximation to the chi-square distribution is adequate. The expression

$$\sqrt{2\chi^2} - \sqrt{2n - 1}$$

is approximately normally distributed as the standard norm distribution. Hence

$$P\left(Z < \chi_n^2(\alpha)\right) = \alpha = \phi\left(\sqrt{2\chi_\alpha^2} - \sqrt{2n - 1}\right)$$

For the 99-percent confidence interval

$$\sqrt{2\chi_n^2(\alpha/2)} - \sqrt{2n-1} = 2.58$$

$$\sqrt{2\chi_n^2(1-\alpha/2)} - \sqrt{2n-1} = -2.58$$

Thus

$$\chi_n^2(1-\alpha/2) = \left[-2.58 + \sqrt{255}\right]^2/2 = 89.6289$$

$$\chi_n^2(\alpha/2) = \left[2.58 + \sqrt{255}\right]^2/2 = 172.0275$$

Consequently, the 99-percent confidence interval for this 128 point example is

$$\left[10\log_{10}\hat{G}(f) + 10\log_{10}\frac{128}{172.0275} < 10\log_{10}\hat{G}(f) < 10\log_{10}\hat{G}(f) + 10\log\frac{128}{89.6289}\right]$$

or

$$\left[10\log_{10}\hat{G}(f) - 1.3\ \text{dB} < 10\log_{10}\hat{G}(f) < 10\log_{10}\hat{G}(f) + 1.5\ \text{dB}\right]$$

BIBLIOGRAPHY

Abdelhamid, A. N., Harrje, D. T., Plett, E. G., and Summerfield, M., "Noise Characteristics of Combustion Augmented High-Speed Jets," AIAA Paper No. 73-189, 1973.

Bendat, J. S. and Piersol, A. G., Random Data: Analysis and Measurement Procedures, Wiley-Interscience, 1971, p. 85.

Bergman, P. G., "The Wave Equation in a Medium With a Variable Index of Refraction," J. Acoust. Soc. Am., Vol. 17, No. 4, April 1946, pp. 329-333.

Bird, R. B., Stewart, W. E., and Lightfoot, E. N., Transport Phenomena, John Wiley, New York, 1960.

Bonnell, Marshall, R. L. and Riecke, G. T., "Combustion Instability in Turbojet and Turbofan Augmentors," AIAA Paper No. 71-698, 1971.

Byron, F. W. and Fuller, R. W., Mathematics of Classical and Quantum Physics, Addison-Wesley Publishing Co., 1970, p. 395.

Candel, S. M., "Acoustic Conservation Principles and an Application to Plane and Modal Propagation in Nozzles and Diffusers," J. Sound Vib., Vol. 41, No. 2, 1975, pp. 207-232.

Chow, J. C. F., "Attenuation of Acoustic Waves in Dilute Emulsions and Suspensions," Journal of the Acoustical Society of America, Vol. 36, December 1964, pp. 2395-2401.

Cole III, J. E. and Dobbins, R. A., "Propagation of Sound Through Atmospheric Fog," Journal of the Atmospheric Sciences, Vol. 27, 1970, pp. 426-434.

Cole III, J. E. and Dobbins, R. A., "Measurements of the Attenuation of Sound in a Warm Air Fog," Journal of the Atmospheric Sciences, Vol. 28, March 1971, pp. 202-209.

Conte, S. D. and deBoor, C., Elementary Numerical Analysis, McGraw-Hill, New York, 1972, pp. 74-83.

Cummings, A., "Sound Generation and Transmission in Flow Ducts With Axial Temperature Gradients," J. Sound Vib., Vol. 57, No. 2, 1978, pp. 262-279.

Davidson, G. A., "Sound Propagation in Fogs," Journal of the Atmospheric Sciences, Vol. 32, November 1975, pp. 2201-2205.

Dobbins, R. A. and Temkin, S., "Propagation of Sound in a Gas Particle Mixture and Acoustic Combustion Instability," AIAA Journal, Vol. 5, 1967, pp. 2182-2186.

Duff, G. F. and Naylor, D., Differential Equations of Applied Mathematics, John Wiley & Son, Inc., 1966, pp. 44-48.

Emmerling, J. J., "Experimental Clean Combustor Program, Phase I, Noise Measurement Addendum." NASA CR-134853 (July 1975).

Emmerling, J. J. and Bekofske, K. L., "Experimental Clean Combustor Program, Phase II, Noise Measurement Addendum," NASA CR-135045 (January 1976).

Epstein, P. S. and Carhart, R. R., "The Absorption of Sound in Suspensions and Emulsions. I. Water Fog in Air," Journal of the Acoustical Society of America, Vol. 25, May 1953, pp. 553-565.

Eversman, W., "Acoustic Energy in Duct, Further Observations," J. Sound Vib., Vol. 62, No. 4, 1979, pp. 571-532.

Faeth, G. M., "Current Status of Droplet and Liquid Combustion," Paper presented at the Combustion Institute, Spring Technical Meeting, Cleveland, Ohio, March 28-30, 1977.

Friedman, B., Principles and Techniques of Applied Mathematics, Wiley, New York, 1956, pp. 164-167.

Goldstein, M. E., Aeroacoustics, McGraw-Hill International Book Co., 1976, pp. 30, 263.

Gouldin, P. C., Combust. Sci. Technol., Vol. 7, 1973, pp. 33-45.

Graves, C. C. and Bahr, D. W., "Atomization and Evaporation of Liquid Fuels," in Basic Considerations in the Combustion of Hydrocarbon Fuels With Air, ed. Barnett, H. C. and Hibbard, R. R., NACA Report 1300, 1959, pp. 1-31.

Harrje, D., ed., "Liquid Propellant Rocket Combustion Instability," NASA SP-194, 1972.

Hurle, I. R., Price, R. B., Sugden, F. R. S., T. M., and Thomas, A., "Sound Emission from Open Turbulent Flames," Proc. Roy. Soc. A, Vol. 303, 1968, pp. 409-427.

Igarashi, J. and Toyama, M., "Fundamentals of Acoustical Silencers. I - Theory and Experiment of Acoustic Low-Pass Filters," Rep. No. 339 Aeronaut. Res. Inst., Univ. of Tokyo, Vol. 24, No. 10, 1958.

Ingard, U. and Singhal, V. K., "Effect of Flow on the Acoustic Resonances of an Open-Ended Duct," J. Acoust. Soc. Am., Vol. 58, No. 4, October 1975, pp. 788-793.

Jones, Robert E., "II. Emissions Reduction Technology Program," in Aircraft Engine Emissions, NASA CP-2021, 1977, pp. 22-23.

Karchmer, A. and Reshotko, M., "Core Noise Source Diagnostics on a Turbofan Engine Using Correlation and Coherence Techniques," NASA TM X-73535, 1976.

Karchmer, A. M., Reshotko, M., and Montegani, F. J., "Measurement of Far Field Combustion Noise From a Turbofan Engine Using Coherence Functions," AIAA Paper No. 77-1277, 1977.

Karchmer, A. M., "Identification and Measurement of Combustion Noise From a Turbofan Engine Using Correlation and Coherence Techniques," Ph.D. Thesis, Case Western Reserve Univ., Cleveland, Ohio, January 1978.

Kazin, S. B. and Emmerling, J. J., "Low-Frequency Core Engine Noise," ASME Paper 74-WA/AERO-2, 1974.

Knott, P. R., "Noise Generated by Turbulent Non-Premixed Flames," AIAA Paper No. 71-732, 1971.

Kraft, R. E. and Wells, W. R., "Adjointness Properties for Differential Systems With Eigenvalue-Dependent Boundary Conditions, With Application to Fluw-Duct Acoustics," J. Acoust. Soc. Am., Vol. 61, No. 4, April 1977, pp. 913-922.

Lampton, M., "Transmission Matrices in Electroacoustics," Acoustica, Vol. 39, 1978, pp. 239-251.

Linden, L. H. and Heywood, J. B., "Smoke Emission From Jet Engines," Combust. Sci. Technol., Vol. 2, 1971, pp. 401-411.

Lumsdaine, E. and Ragab, S., "Effect of Flow on Quasi-One-Dimensional Acoustic Wave Propagation in a Variable Area Duct of Finite Size," J. Sound. Vib., Vol. 53, No. 1, 1977, pp. 47-61.

Lumsdaine, E., "Calculation of Pressure Reflection Ratio," J. Sound Vib., Vol. 52, No. 1, 1977, pp. 145-147.

Maling, G. C., "Simplified Analysis of Rijke Phenomenon," Journal of the Acoustical Society of America, Vol. 35, 1963, p. 1058.

Mani, R., "Discrete Frequency Noise Generation From an Axial Flow Fan Blade Row," ASME Trans., Journal of Basic Engineering, Vol. 92, 1970, pp. 37-43.

Marble, F. E., "Some Gasdynamic Problems in the Flow of Condensing Vapor," Astronautica Acta, Vol. 14, 1969, pp. 585-614.

Marble, F. E. and Wooten, D. C., "Sound Attenuation in a Condensing Vapor," The Physics of Fluids, Vol. 13, No. 11, November 1970, pp. 2657-2664.

Marble, F. E. and Candel, S. M., "Acoustic Attenuation in Fans and Ducts by Vaporization of Liquid Droplets," AIAA Journal, Vol. 13, No. 5, May 1975, pp. 634-639.

Mathews, D. C. and Rekos, Jr., N. F., "Direct Combustion Generated Noise in Turbopropulsion Systems Prediction and Measurement," AIAA Paper No. 76-579, 1976.

Mechel, von F., Schilz, W., and Dietz, J., "Akustische Impedanz Einer Luftdurchstromten Offnug," Acustica, Vol. 15, 1965, pp. 199-206.

Miwa, T. and Igarashi, J., "Fundamentals of Acoustical Silencers. II - Determination of Four Terminal Constants of Acoustical Elements," Rep. No. 344. Aeronaut. Res. Inst., Univ. of Tokyo, Vol. 25, No. 4, 1959.

Möhring, W., "Energy Flux in Duct Flow," J. Sound Vib., Vol. 18, No. 1, 1971, pp. 101-109.

Morfey, C. L., "Sound Transmission and Generation in Ducts With Flow," J. Sound Vib., Vol. 14, No. 1, 1971, pp. 37-55.

Morfey, C. L., "Acoustic Energy in Non-Uniform Flows," J. Sound Vib., Vol. 14, No. 2, 1971, pp. 159-170.

Morse, M. P. and Feshbach, H., Methods of Theoretical Physics, McGraw-Hill Book Company, 1953, p. 793.

Mungur, P. and Plumblee, Jr., H. E., "Influence of the Jet Exhaust Flow Field on the Acoustic Radiation Impedance of a Jet Pipe Opening," AIAA Paper No. 79-0676, March 1979.

Muthukrishnan, M., Strahle, W. C., and Handley, J. C., "Effect of Conical Flameholders on Combustion-Generated Noise," AIAA Journal, Vol. 14, No. 8, 1976, pp. 995-996.

Norgren, C. T., "Determination of Primary-Zone Smoke Concentrations From Spectral Radiance Measurements in Gas Turbine Combustors," NASA TN D-6410, 1971.

Parrott, Tony L., "An Improved Method for Design of Expansion Chamber Mufflers With Application to an Operational Helicopter," NASA TN D-7309, 1973.

Plett, E. G., Leshner, M. D., and Summerfield, M., "Combustion Intensity and Distribution Relation to Noise Generation," AIAA Paper No. 75-524, 1975.

Polis, M. P. and Goodsen, R. E., "Parameter Identification in Distributed Systems: A Synthesizing Overview," Proceedings of the IEEE, Vol. 64, No. 1, January 1976, pp. 45-61.

Reshotko, M. and Karchmer, A., "Combustor Fluctuating Pressure Measurements In-Engine and in a Component Test Facility - A Preliminary Comparison," NASA TM-73845, 1977.

Reshotko, M., Karchmer, A., Penko, P. F., and McArdle, J. G., "Core Noise Measurements on a YF-102 Turbofan Engine," AIAA Paper No. 77-21, 1977.

Shivashankara, B. N., "Gas Turbine Engine Core Noise Source Isolation by Internal-to-Farfield Correlations," AIAA Paper No. 77-1276, 1977.

Simons, G. A. and Lewis, P. F., "Mass Transport and Heterogeneous Reactions in Porous Medium," Paper presented at the Combustion Institute, Spring Technical Meeting, Cleveland, Ohio, March 28-30, 1977.

Smith, T. J. B. and Kilham, J. K., "Noise Generation by Open Turbulent Flames," The Journal of the Acoustical Society of America, Vol. 35, No. 5, May 1963, pp. 715-724.

Sofrin, T. G. and Ross, D. A., "Experimental Clean Combustor Program, Phase I, Noise Addendum," NASA CR-134820 (October 1975).

Sofrin, T. G. and Riloff, Jr., N., "Experimental Clean Combustor Program - Noise Study," NASA CR-135106 (September 1976).

Stewart, W. L. and Weber, R. J., "A Review of NASA's Propulsion Programs for Civil Aviation," AIAA Paper No. 78-43, 1978.

Stone, J. R., "On the Effects of Flight on Jet Engine Exhaust Noise," NASA TM X-71819, 1975.

Strahle, W. C., Muthukrishnan, M., and Neale, D. H., "Coherence Between Internal and External Noise Generated by Gas Turbine Combustors," AIAA Paper No. 77-20, 1977.

Strahle, W. C., Muthukrishnan, M., and Neale, D. H., "Experimental and Analytical Separation of Hydrodynamic, Entropy and Direct Combustion Noise in a Gas Turbine Combustor," AIAA Paper No. 77-1275, 1977.

Swinbanks, M. A., "The Sound Field Generated by a Source Distribution in a Long Duct Carrying Sheared Flow," J. Sound Vib., Vol. 40, No. 1, 1975, pp. 51-76.

Takahashi, Y., Robins, M. J., and Auslander, D. M., Control and Dynamic Systems, Addison-Wesley Publishing Co., 1972, p. 266.

Temkin, S. and Dobbins, R. A., "Attenuation and Dispersion by Particulate-Relaxation Processes," Journal of the Acoustical Society of America, Vol. 40, No. 2, 1966, pp. 317-324.

Tester, B. J., "Acoustic Energy Flow in Lined Ducts Containing Uniform Flow," J. Sound Vib., Vol. 28, No. 2, 1973, pp. 205-215.

von Glahn, U. H., "Correlation of Combustor Acoustic Power Levels Inferred From Internal Fluctuating Pressure Measurements," NASA TM-78986, 1978.

Welty, J. R., Wicks, C. E., and Wilson, R. E., Fundamentals of Momentum, Heat and Mass Transfer, John Wiley, New York, 1969.

Wright, F., "The Oxidation of Soot by O Atoms," International Symposium on Combustion, 15th (Combustion Institute, Pittsburgh, Pa., 1975), pp. 1449-1459.